UNIVERSITY OF TARTU
Faculty of Science and Technology
Institute of Technology

Mark Merzlikin

Electrochemical sensing on flexible carbon electrodes for application in soft robotics

Bachelor's Thesis (12 ECTS)

Curriculum: Science and Technology

Supervisors:
Dr. Janno Torop
Dr. Ausra Baradoke

Tartu 2021

Electrochemical sensing on flexible carbon electrodes for application in soft robotics

Abstract:

Commercially available carbon fibers and composites made of commercially available activated carbon and κ-carrageenan were tested as prospective materials for manufacture of biocompatible soft actuators using electrochemistry and scanning electron microscopy.

Keywords:

Carbon fibers, carrageenan, dopamine, soft robotics.

CERCS

T390 Polymer technology, biopolymers

Paindlike süsinikkiudude abiga elektrokeemiline seire pehmerobootika kasutamiseks

Lühikokkuvõtte:

Kaubandusest saadavad süsinikkiud ja kaubandusest saadavast aktiivsöest ja kapa-karrageenist tehtud komposiidid olid testitud loodetavateks materiaalideks biokokkusobivate pehmeaktuaatoride tootmiseks elektrokeemia ja elektromikroskoopia kasutamas.

Võtmesõnad:

Süsinikkiud, karrageen, dopamiin, pehmerobootika.

CERCS

T390 Polümeeride tehnoloogia, biopolümeerid

AKNOWLEDGMENTS

First of all, I would like to thank my supervisors Dr. Janno Torop and Dr. Ausra Baradoke for their guiding and crucial advice during my research at University of Tartu. I also thank the Intelligent Materials and Systems Lab for providing me the possibility to make thesis work. I thank Ali Jafarov and Alexandra Elsakova for their training and assistance with the experimental analysis of the CFMB electrodes and the crucial part they played in the design and production of the 3D-printed electrochemical cell used in this work. Also, I am grateful for useful discussions provided by Dr. Indrek Must and Dr. Urmas Johanson.

TABLE OF CONTENTS

TERMS, ABBREVIATIONS AND NOTATIONS

WE – Working electrode

CE – Counter electrode

RE – Reference electrode

k-car/κ-car – κ-carrageenan

CV – Cyclic voltammetry

EIS – Electrochemical impedance spectroscopy

EDL – Electrical double layer

CF – Carbon fiber(s)

CFMB – Carbon fiber microbundle

EDLC – Electrical double-layer capacitor

PB – Phosphate buffer

PBS – Phosphate-buffered saline

$\mathbf{E_{pa}}$ – Peak anodic potential

$\mathbf{E_{pc}}$ – Peak cathodic potential

$\mathbf{I_{pa}}$ – Peak anodic current

$\mathbf{I_{pc}}$ **–** Peak cathodic current

$\mathbf{E_{1/2}}$ – half-wave potential

$\mathbf{E_p}$ – peak-to-peak separation

RR% - relative response in percents

INTRODUCTION

Soft robotics is a prospective field of research, with results promising custom-shaped actuators well-purposed for safe physical contact, usable in invasive procedures on living beings, handling of fragile objects and a potential to be designed with biomimicry in mind. This makes them perfect candidates for actuated prosthetics or even creation of artificial muscles. Such applications on the border of robotics and biology would require biocompatibility and an interface for the neural control of movement, with such systems sometimes classified as the field of study of neurorobotics. Detection of a neurotransmitter, such as dopamine, is usually realized by the means of biosensors, with one of the most prominent examples of such being carbon fiber microelectrodes. Carrageenans are a family of algae-derived polysaccharides with a curious ability to gelate under the influence of cations. Their complete biocompatibility and biosustainable origins would make them good candidates for actuator materials, should such an ability be made reversible on demand.

In this work, commercially available carbon fiber microbundles were tested as candidates for dopamine biosensing in pure, unmodified forms and, following the widespread practice of carbon fiber surface functionalization, tested as potential substrates for modification with carrageenan-bound carbon ink. 3D printed electrochemical cells were designed and used to account for structural specifics of the carbon fibers. The composite films made of carbon-carrageenan inks were created and characterized using electrochemistry and electron microscopy.

1 LITERATURE OVERVIEW

1.1 Carrageenans

Carrageenans are a family of linear sulfated polygalactans obtained from various red algae species. These biopolymers are able to easily form aqueous gels with good physical properties and find many applications in food (e.g., as thickeners or for production of jelly), beauty industry (e.g. toothpaste, shaving and face creams, both as a thickener, nutrient source and due to its alleged antibacterial properties[1]) as well as in pharmaceutics (e.g. the basis for pills[2,3]). Availability from natural sources and biocompatibility of carrageenans makes them an object of studies for prospective usage in various spheres, especially in medicine[4,5] and as smart[6,7] and high-tech[8–10] materials[11].

The common structural pattern of the carrageenans consists of a repeating disaccharide made of α-1,4-linked D-galactopyranose and β-1,3-linked D-galactopyranose, with the former also possibly replaced by α-1,4-linked 3,6-anhydro-D-galactopyranose[2,3]. Generally, carrageenans are divided into six forms, named with various Greek letters: lambda (λ), kappa (κ), iota (ι), mu (μ), nu (ν) and theta (θ), of which the first three (***Fig. 1***) are used commercially most prevalently[2]. All of these are mainly differentiated by their content of 3,6-D-anhydrous-D-galactose and sulphate ester group positions on the disaccharide monomer, as well as the group amount[3]. The presence of negatively charged organic sulphate groups gives the polymer anionic properties, which can help in developing carrageenan-based drug delivery systems[12] or polyelectrolyte membrane nanocoatings[4].

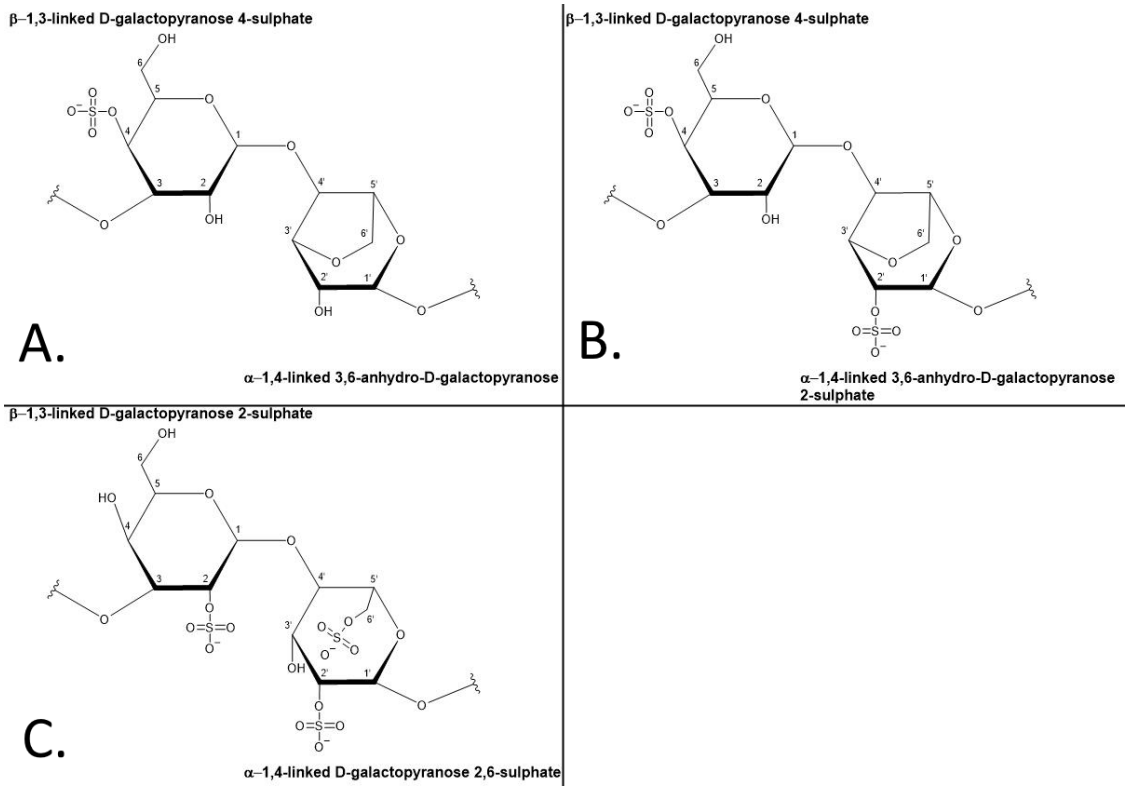

Figure 1. *Chemical structure of the disaccharide monomers of* ***A.*** *κ,* ***B.*** *ι, and* ***C.*** *λ carrageenans. In this work, κ-carrageenan was used most extensively.*

1.2 Carrageenan gels

Of interest is a property of carrageenans given by the sulphate groups; their ability to aggregate around positively charged ions. The aggregation causes the polysaccharide/water mixes to undergo quick and intensive gelation, forming stronger, more elastic gels[13] with as much as the introduction of the cations, usually in form of salt solutions. The ions traditionally used for such gelation are metal cations, like K^+ and similar monovalent ions except for Li^+ and Na^+, which are thought to form less-stable aggregations due to shielding effects of excessive size[13,14]. Nevertheless, divalent ions such as Ca^{2+} are also usable for these purposes[13], as well as some trivalent ions (like Fe^{3+})[14,15]. κ-carrageenan was reported to be gelating better with monovalent ions, forming sort of a superstrand structure[16], while ι-carrageenan has a higher affinity for divalent ions (namely, Ca^{2+})[15]. However, there also exist reports of this not being the case, as κ-carrageenan was also found to form quite rigid gels due to Ca^{2+} ions (and even forming superstrand-like structure)[13] and was also found able to gelate under the influence of Fe^{3+} ion[15]. It was reported that critical gel strength increases with increasing Ca^{2+} concentration, both on its own and when normalized to Ca^{2+} concentration to , ranging from approximately 1.35 to 5.5 Pa x s^n at 0.1 and 0.4 mM Ca^{2+} for critical gel strength and approximately 13 to 13.8 Pa x s^n/mM for 0.1 and 0.4 mM Ca^{2+} for normalized gel strength, with *n* being stress relaxation component used for characterizing the stress relaxation rate (the inverse of the frequency at which storage

(elastic) and loss (viscous) components of a complex rheological modulus reach equal values when the gel is subjected to stress at varied frequencies) of the gel at the gelation point. For 0.1 mM Ca^{2+}, *n* was reported to have the value of approximately 0.65 while for 0.4 mM Ca^{2+} it was around 0.51[17]. All the values were reported for 2% w/w κ-car/water mixes.

Altogether, even though the ion-induced gelation has contributed to the usefulness of carrageenan for many years, its more practical details are surrounded with conflicting reports. It might be possible that this deficiency of insight is at least partially caused by carrageenan seemingly being mostly present as a research topic in food journals alone (though there is indeed a general positive trend for the number of scientific papers on carrageenan, and it has greatly increased since the 90s[1]).

However, the exact mechanism of the ion-induced gelation is not clear[18], though there has been a lot of research into the subject. At the same time, there exist models providing schematic descriptions and predicting the structure of the final aggregations, the most favoured of which nowadays is domain model[19]. It describes the aggregation as a three-step process (***Fig. 2***), where the 'disordered' polysaccharide coil chains first transform into 'ordered' helical forms followed by pairing into double helices, with sulphate groups oriented to the outside on each chain to negate repelling forces. The last step is the final aggregation, when the double helices unite in pairs around the cations which serve as the connection interacting with the negative sulphate groups.

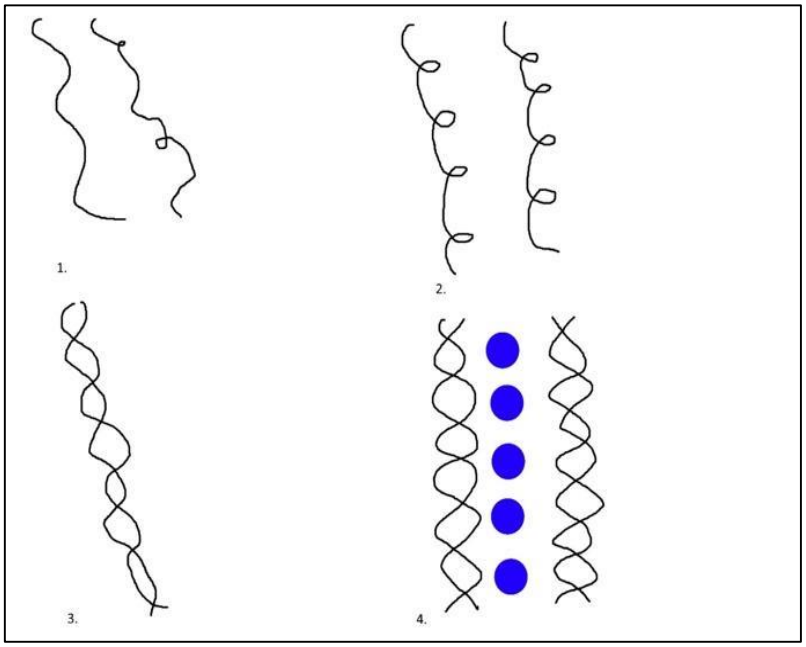

Figure 2. *The scheme of the steps of the domain model for cation-induced carrageenan aggregation.* ***1****. Disordered carrageenan strands.* ***2****. Ordered carrageenan coils.* ***3****. The double-helical aggregation of carrageenan.* ***4****. The final structure of the gel; double helices united by cations.*

1.3 Research motivation

If a way to controllably reverse this process was found, it could contribute to the creation of a kind of a variable-viscosity material, which would find use both as some material with changing friction, useful for the moving structural components like bearings[20] or as a basis for some actuator. Soft-bodied actuators, their design, production and study are generalized as soft robotics, a subsphere of common robotics. Soft robots are attracting more and more interest due to much bigger variety of possible forms and sizes, bigger effectivity because of a better energy output to weight ratio[21], easier storage thanks to pliable materials, ability of safer interactions with fragile bodies or even living tissue, not even mentioning general biomimicry[22] of such robots making them more 'organic' with potential for aesthetic use. Additionally, easily-made carrageenan coatings could be of interest, should they prove to be conductive or should they serve as basis for further functionalization, to the ends of bioanalysis, especially in light of recent insights into similar hydrogel coatings coatings[23].

The Ca^{2+} ions applicable for the gelation of carrageenans are crucial triggers in neurotransmitter release, realized through synaptogmin proteins and regulated by the action potentials in the presynapse terminal[24,25], with a multi-role function in the process[26]. K^+ ions, the most traditional cation type used for the gelation process, are also reported to have influence on neurotransmitter activity, namely, seemingly regulating the frequency of the activation of neurons[27] and controlling presynaptic activity spikes, in particular, through the influence on Ca^{2+} flux[28].

In soft robotics, dopamine, a type of a neurotransmitter, was most extensively used as a functional coating to achieve sensitivity[29] and to provide adhesive functions (as polydopamine)[30]. At the same time, possibilities of neuron-like systems in robotics, possessing prospect of learning, adaptability and general flexibility of a real brain[31], are always of interest, with various attempts to realize learning robotic systems already existing[32,33]. Systems based on principles adjacent to the function of dopamine in the brain are also considered, like reward-modulated learning systems where some signal is associated with positive reinforcement of behavior[34] (e.g., situational spiking used to teach a spiking neural-network controlled robot to choose the most rewarding behavior and adapt as the most rewarding behavior changed[35]) or actor-critic reinforcement learning where delayed feedback is received as a consequence of environmental interactions (with reward-like response allowing to affect the network analogous with long-term effects of dopamine reward-like response in human brain)[31,36].

An actuator design utilizing current-controllable Ca^{2+} or K^+ flux could thus potentially provide a basis for prospective biocompatible robots, prosthetics or artificial muscles integrated into the

native signaling system of nervous cells. Such a design would have even more prominence should an ability for neurotransmitter sensing be incorporated into it, as it would allow for creation of direct non-simulated self-learning robotic systems. With carrageenan, calcium and potassium ions already having biosustainable origins and being obtainable from conventional sources, the best consideration for the biosensor would be a cheap biocompatible material as well.

1.4 Carbon fibres

Carbon fibres (CF) are prized for their relative chemical inertness as well as good electrical and mechanical properties[37]. Even since the late 1970s, they have been known as a promising electrode material for biosensing and other electrophysiological applications[38] with miniaturization perspectives allowing *in vivo* analysis[37,39–42], further supported by their lack of toxicity to cells[40], while their sensitivity enables the studies to be performed extracellularly on par with the best tungsten electrodes[37,38]. Carbon-fibre derived materials have also been utilized as electrodes for supercapacitors[43] and fuel cells[44].

A traditional structure of a CF-electrode is a single fibre threaded through an insulating tube, usually made of borosilicate glass or some plastic[37,39], potentially, with a pipette puller[38,39]. In original designs, one possible method of fabrication of the contact for the electrode was filling the top side of the tube containing the fibre with a mix of graphite powder and polyester resin, the resin alone being present at the bottom end of the capillary to provide insulation. A contact was then pushed into the filled capillary as far as possible, and the electrode was left for 24 hours to let the filling dry[39]. Another method was to fill the top of the electrode tube with a saline solution and dip an Ag/AgCl wire into it for contact[38]. Some other way is gluing the fibre with a conductive wire using some conductive paint or silver-filled epoxy glue[37]. After the fibre is pulled through the supporting tube, a sizable part of it is usually left protruding from the bottom tip (or it is left unable to go through fully, depending on the narrowness of the tip). In that case, the fibre is additionally trimmed to some smaller length, either by using microscissors, electrochemical etching in some alkali or chromic acid or by spark etching[37,45]. If the fibre is blocked by the tube itself, only the supporting material is cut[39]. The design might include additional glass capillaries by the side of the tube containing the fibre, which can be used to deliver some drugs or reagents into the studied sample (for example, using iontophoresis)[37,46].

CF-electrode biosensors have been applied for detection of various neurotransmitters, particularly, catecholamines (dopamine, serotonin, norepinephrine etc)[39] as well as other oxidizable biochemical species and nervous system messengers, such as hydrogen peroxide[47]

or nitric oxide (NO)[48]. Although mentioned biomolecules are important signalling species in living organisms[49], their activity may sometimes also serve as an indicator of some neurological disease[50–53], sometimes indirectly (such as the NO-dependent endothelium-derived relaxing factor[54,55] being associated with multiple diseases)[56–59]. There are also some studies of immunosensors made from the modified carbon fibre electrodes[60].

In conjunction with the aforementioned *in vivo* analysis abilities, there are great prospects of CF-electrode application in neurobiological studies as well as drug testing[37,40,61] or maybe, in perspective, medical treatments (both as biosensors[62–64] and due to their physical properties[65–67]). The fast-scan cyclic voltammetry (FSCV) is nowadays considered to be the most advantageous and wide-used technique for neurotransmitter detection *in vivo*[40,61] (though constant-potential amperometry, chronoamperometry and some other electrochemical methods are also used[37,40]), as it allows both fast detection and identification of analyte[68,69] while maintaining some selectivity. Particularly, the latter is an often concern as there are many electroactive species present *in vivo*[61], so the search for various selectivity-increasing modification is a frequent study topic[37,40,61]. A possible disadvantage of CF-biosensors are low response currents[70].

Classical modifications are the coating of the fibre surface with some ion-selective polymers, with Nafion[71] or overoxidized polypyrrole films[72,73] being traditional. Another classic method of interest is an electrochemical treatment where a CF-electrode submerged into PBS is cathodized by applying an alternating triangle-wave potential (from 0 to +3 V) to it with a frequency of 70 Hz[42,74]. Nevertheless, all these methods tend to increase response times, complicating potentiometric analysis[71,73], with the electrochemical methods promoting adsorption[75]. Thus, uncoated fibres can still be used where the short response times are of the essence[61].

As the search for better modifications continues, attempts were made to use polysaccharides[60], platinum[41] or polydopamine[76], as well as considerations of hybrid carbon materials, with the latter claimed to be the least investigated materials[77], though there were indeed studies of CF-biosensors combined with carbon nanotubes[70,78–81], producing seemingly stable biosensors with improved conductivity and surface area[70] which were applicable for FSCV.

1.5 Electrochemistry

In general, electrochemistry refers to the area of chemistry which concerns charge separation and transfer processes[82]. In practice, electrochemical setups usually include electrodes forming

a closed circuit with the studied material, often in the form of a solution of some ions. The electrodes have different compositions and structures, limiting them to specific functions and defining their properties in a setup.

The most basic electrochemical cell (an apparatus containing the electrodes and the analysed material in the form of an electrolyte or an electrode) consists of two electrodes: the working electrode (WE, also known as the indicator electrode), the processes on which are investigated through the controlled changes of its potential or current; and the auxiliary electrode (also known as the counter electrode, CE), which is used to complete the circuit. In such a scheme, however, the CE also serves as a reference for the cell's potential, which can lead to the instability of that potential[82]. So, nowadays, the most used setup is a three-electrode system, which is valued for its ability to allow to distribute the reference and counter roles between two electrodes[82].

1.6 Cyclic Voltammetry

Cyclic voltammetry (CV) is an electrochemical analysis technique where the potential of the working electrode is linearly varied between two set voltages with a set rate, while the generated current is measured (***Fig 3.***). The method is used to study reduction and oxidation processes of some molecules, as well as electron transfer-initiated chemical reactions. The result of a CV scan is a voltammogram, a graph of current versus voltage. In case of electrically conducting charging species the voltammogram depicts a background hysteresis with peaks corresponding to charge transfers (oxidations and reductions of the analysed species, relative to the potential).

For high, positive potentials, the resulting peaks are called anodic and the potential corresponding to the tip of such a peak is peak anodic potential, E_{pa}. Likewise, a peak at low, negative potentials is called cathodic peak (with peak cathodic potential, E_{pc}, marking its tip). The heights of peaks are then, similarly, peak cathodic and anodic currents, taken as heights of the peaks from the tip to the background current, the latter taken into consideration to account for capacitance of Electrical double layer (EDL).

One of the ways to characterize a redox reaction happening due to a triangle-wave sweep is a half-wave potential ($E_{1/2}$), which is a potential marking a middle point between the peaks of a cathodic and an anodic wave for a single electroactive species. If the peak potentials are known, it can be calculated as follows:

$$E_{1/2} = |E_{pa}| - (|E_{pa}| + |E_{pc}|)/2$$

Another similar way is to consider the separation of the cathodic and anodic wave through the potential distance between the peaks, called peak-to-peak separation (E_p).

Separation of oxidation and reduction peaks for the same species, peak currents, half-wave potentials and their dependence on scan rate and its derivatives can be used to check chemical reversibility of the studied reaction, derive diffusion coefficient of the analyte or the active area of the electrode[83].

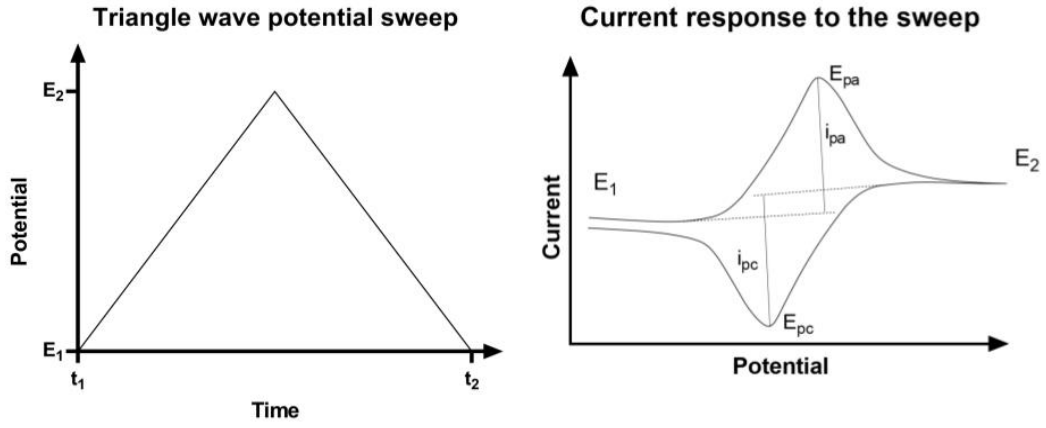

***Figure 3 On the left**: the triangle potential sweep wave applied during one cycle of the CV analysis. t_1 and t_2 are the beginning and ending times of the cycle, respectively, while E_2 and E_1 are the maximal and minimal potentials applied during the sweep. **On the right:** the current generated as the function of the triangle sweep voltage; a voltammogram. The potential window here is the same as in the graph on the left: E_1 to E_2.*

1.7 Electrochemical Impedance Spectroscopy

Electrochemical Impedance Spectroscopy (EIS) is a method of electrochemical analysis where the studied object is exposed to a sinusoidal AC voltage of some set amplitude and changing frequency and the current, which varies in amplitude and phase with the voltage, is measured (***Fig. 4***)[84]. The gained in-phase current then determines the real (resistive) component of impedance, and the out-of-phase one determines the imaginary (capacitive) component of the impedance, the complex resistance of circuit (and here, of the sample) to the electrical current inside it[85].

The existence of impedance as a parameter is necessitated by the fact that in real AC circuits resistance varies with frequency and the current and voltage are not in phase, as capacitive and inductive effects are present due to the latter[86]. For EIS, most popular forms of measured data are Nyquist plots (***Fig. 5***), with real and imaginary impedance components plotted against each other[5], or Bode plots (***Fig. 7***), where logarithm of the absolute value of impedance and the phase angle are plotted separately versus the logarithm of frequency[85].

Nyquist plots are also sometimes alternatively named Cole-Cole plots, though the latter is more often associated with plots of dielectric constants or capacitance, which retain the general shape and real vs imaginary plotting setting of Nyquist plots (***Fig. 6***).

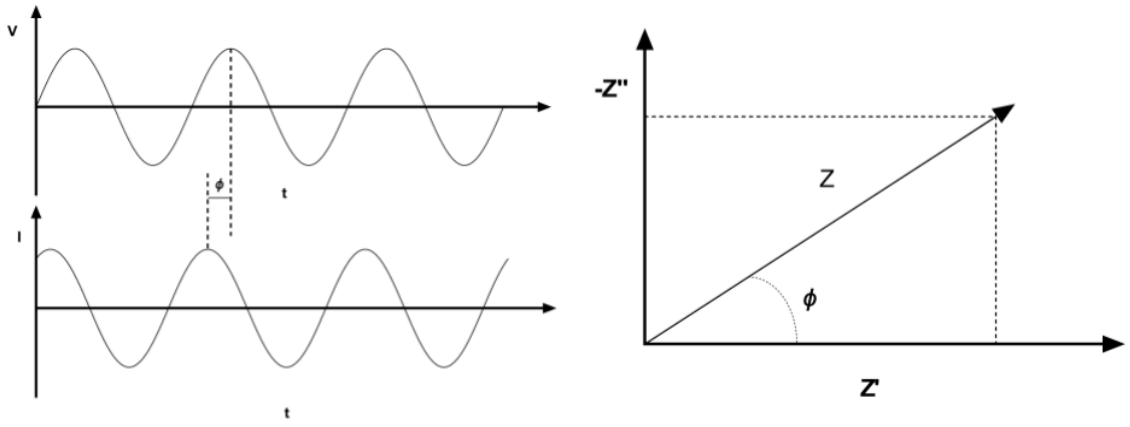

Figure 4. On the left: *the supplied voltage (V) is oscillating with some constant frequency and amplitude about the steady state (x-axis), with the current response (I) lagging behind the voltage by some phase shift (ϕ).* ***On the right:*** *a complex resistance response for a single frequency: real (x-axis) and imaginary (y-axis) components form the total impedance modulus with the angle between the latter and the x-axis being the phase shift.*

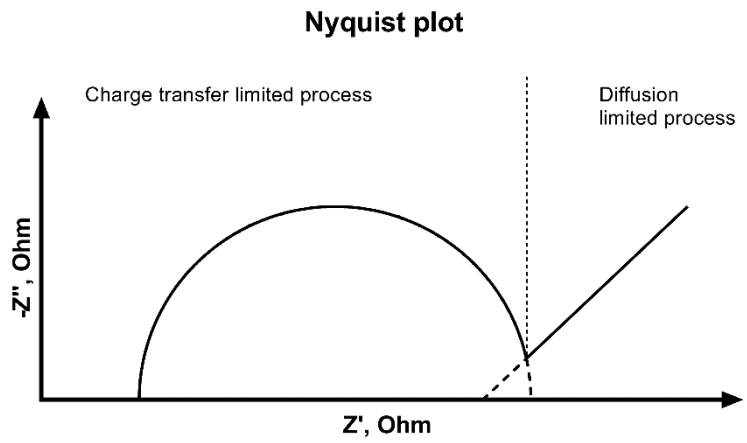

Figure 5. *An ideal example of a Nyquist plot. The frequency of the steady-state centered oscillation increases from right to left. The system here shows a capacitor-like (diffusion-limited) response on low frequencies, while at high frequencies it is analogous to a resistor and a capacitor connected in parallel (charge-transfer limited).*

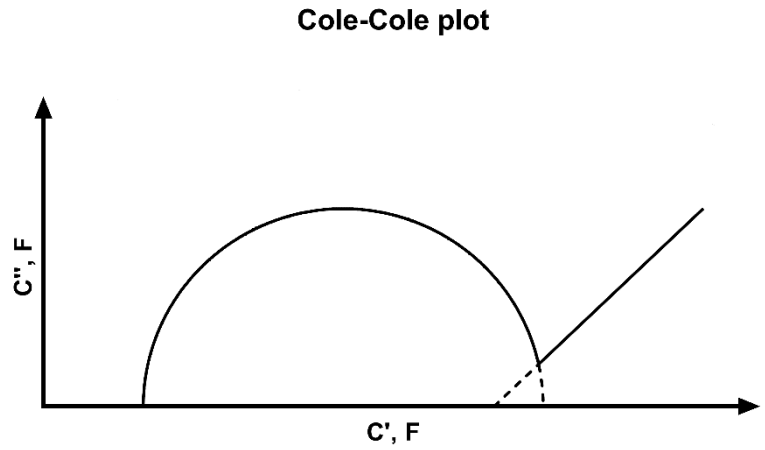

Figure 6. *An idealized Cole-Cole plot for capacitance, with the frequency of the oscillation increasing from right to left, as in a Nyquist plot. C' and C'' can be connected to real and pseudocapacitance (rapid reversible Faradaic reactions).*

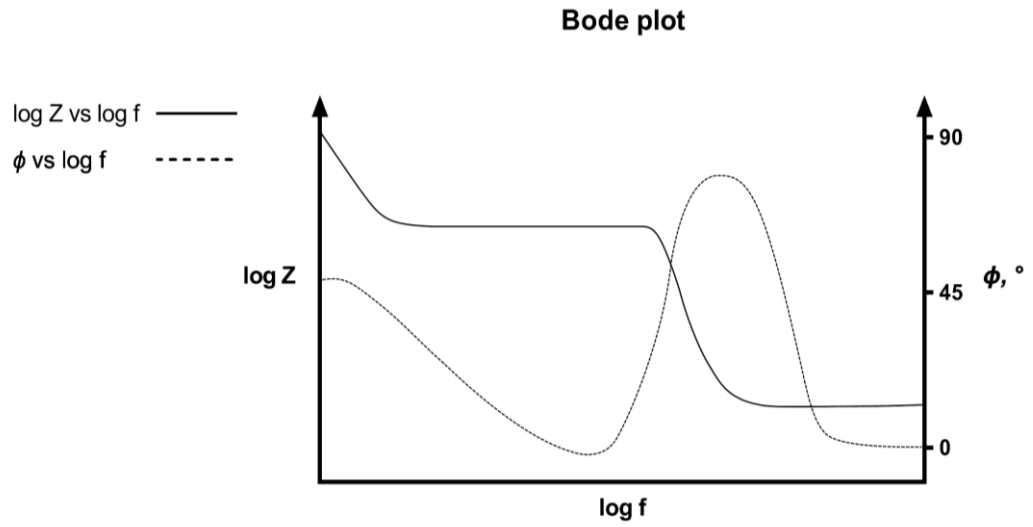

Figure 7. *An idealized example of a Bode plot. In these data presentations two charts are provided at once, one for the logarithm of the total impedance of a system and one for the phase angle response, both plotted versus the logarithm of either the frequency or the angular frequency of the voltage.*

EIS is used to determine various parameters of electrochemical systems, such as double-layer capacitance, exchange-current density, charge-transfer resistance etc[87]. It is used in food industry for pathogen detection[88], corrosion analysis[89] and studies of battery[44], fuel cell[90] and supercapacitor[91] properties.

1.8 Scanning Electron Microscopy

Scanning Electron Microscopy (SEM) is a method of electronic microscopy which generates an image based on radiation emitted from a sample as it is subjected to a thin electron ray. Electrons are emitted from an electron gun onto the surface of some studied specimen, after which the beam is transformed into a thinner probe ray used to scan the select area of the sample. The electrons disperse in the sample's surface in an onion-like form which dimensions depend on the atomic composition of the sample and the energy of the beam[92,93]. As the studied object is subjected to the electron ray, various physical interactions happen which lead to different results; electron scattering and Bremsstrahlung, X-ray emissions, electron backscattering, emissions of secondary electrons, Auger electron emissions etc. Many of these can be detected and used to picture the surface of the sample, creating a highly magnified and detailed image of it (with spatial resolution of up to tens of Angstroms).

1.9 Energy-dispersive X-ray spectroscopy

Energy-dispersive X-ray spectroscopy (EDS or EDX) is an atomic spectroscopy method which utilises X-ray emissions to determine the composition of a sample. In EDX, an electron ray is used to bombard the studied material which leads to a displacement of lower-energy electrons from the sample's inner atomic shells; higher-energy inner shell electrons then move in to replace then, ejecting a big amount of energy in form of X-rays. The emitted quants are specific for every element[92]. Being an energy-dispersive method, EDX utilized digital analysis of the emissions; all the X-ray waves are first gathered by a semiconductor detector and then transformed into voltage signals of different magnitudes. EDX systems are often coupled with SEM devices, as the underlying principles of operations for both are almost identical, especially the scanning process[92,93].

2 RESEARCH OBJECTIVES AND TASKS

The objective of this thesis was to investigate potential use of electrochemical sensing systems and biomaterials for potential application in soft robotics. The following tasks were established to achieve the objective:

2.1. To design and fabricate an electrochemical cell for flexible high area electrodes using biocompatible or biodegradable materials and 3D printing.

2.2. To characterise flexible high area electrodes using microscopy and electrochemistry.

2.3. To characterise flexible high area electrodes for biosensing of physiological analyte, e.g., dopamine in a neutral pH buffer.

2.4. To investigate the existence of significant rapid reversibility of metal cation-induced gelation of κ-carrageenan/water mixes and possibility of controlling it utilizing varied-direction current.

2.5. To investigate the possibility of creating green conductive composites from κ-carrageenan and activated carbon and manufacture samples of such.

2.6. To characterize the conductive composites made from κ-carrageenan and activated carbon using microscopy and electrochemistry.

2.7. To design a soft actuator sample utilizing the κ-carrageenan/activated carbon conductive composites and their elasticity changes due to reversible gelation.

3 EXPERIMENTAL PART

3.1 MATERIALS AND METHODS

3.1.1 Materials and solutions

All reagents were of analytical grade and used without further purification. Aqueous solutions were prepared in milli-P and milli-Q water (18.2 MΩcm). All the experiments were carried out at room temperature 20 ± 2 °C.

Materials for the fabrication of electrodes

Carbon fiber (SIGRAFIL®C30 T050 EPY 382-000A/50k/3300 with 1 percent epoxy size agent) was used for the creation of large carbon fiber microbundle (CFMB) electrodes.

Materials for fabrication of flexible electrochemical cell

The NinjaFlex (United States) filament was used for 3D printing of an electrochemical cell cap.

Reagents for electrochemical analysis

To create a neutral pH environment, phosphate buffer (PB) was made from aqueous 0.2 M monobasic $NaHPO_4$ and 0.2 M dibasic Na_2HPO_4 (Sigma Aldrich, both) solutions, later diluted to 0.1 M of total concentration using mQ water. 2.5 and 5 mM $[Fe(CN)_6]^{3-/4-}$ solutions were made by mixing $Na_4Fe(CN)_6 \cdot 10H_2O$ and $K_3Fe(CN)_6$ (Sigma Aldrich, both) and isolated from light using tin foil. For CF characterization, dopamine solutions were prepared using dopamine hydrochloride (Alfa Aesar) dissolved freshly in PB before each measurement to prevent self-oxidation. The total amounts of dopamine used for analysis were gradually increased in step of 10 from 0 to 100 μM.

Materials for fabrication of carrageenan films

Activated carbon (Vendor Fantomkol, CBF Drinkit AB, Sweden; 0.4-0.85 mm grain size, 1100 m^2/g adsorption area), κ-carrageenan powder, calcium chloride (II) and potassium sulphate (II) solutions (0.5 and 0.45 M) milli-P and milli-Q water, previously-made ~1% carrageenan/water mixture available from an older project of Dr. Torop.

3.1.2 Making a flexible electrochemical cell

The electrochemical cell was built using a 3D printed cap designed for CFMB electrodes. The electrochemical cell had six channels, which prevented flexible CFMB electrodes from interacting. Two additional cavity units designed with a 6 mm diameter for reference and

counter electrodes were present. The filament was printed with the extrusion temperature of 240 Celsius and bed temperature of 50 Celsius. The printing speed was optimized to be 20 mm/s with a 0.2 mm slice having a total printer time of 2 hours. The cell was used to fix the fragility of the CFMB electrode fibers and increase the reproducibility of the tests.

3.1.3 Methodology for electrochemical characterisation of carbon electrodes

The electrodes for electrochemical character have been embedded in a 3D printed cell for electrochemical characterisation. Biologic BP-300 electrochemical laboratory was used to perform the measurements utilizing platinum grid or CFMB as the counter and an Ag/AgCl/(3M KCl) as the reference electrodes.

3.1.4 Making carrageenan/carbon composites

To test the simplicity of the mixing of activated carbon and carrageenan, an attempt to create carbon ink-like mixtures was made. Two samples were made by adding a pre-available ~1% (w/w) mixture of water and κ-carrageenan and the activated carbon powder in glass beakers, with activated carbon additionally crushed in advance using a mortar. All the samples were mixed in a weight ratio of 1:1 (calculated for κ-carrageenan content of the mixture).

The samples were mixed using magnetic stirring beads on 60 Celsius overnight. Both samples turned out seemingly well-mixed, although there was no success in achieving the proper mixing of carrageenan and uncrushed carbon in the future. At the same time, a 0.5 M solution of $CaCl_2$ was made using milli-P water. The carbon-carrageenan mixtures were poured into molds chosen out of convenience (a rectangular Teflon shape and a Petri dish) and thoroughly covered with the chloride solution using a dropper. As expected, this led to quick thickening, resulting in elastic wet slabs of carbon/carrageenan hydrogel composite. Unfortunately, due to the lack of foresight, the samples were not covered as they were left overnight to see if any additional curing would take place, and dried, turning into thin flexible black films with slight proneness to crumbling.

3.1.5 Checking the presence of a visible elasticity response

Following through with the original assumption of easy current-inducible elasticity changes in carrageenan hydrogels, simple setups made of woven carbon threads connected using a $CaCl_2$ solution-cured hydrogel layer were subjected to triangle-wave sweeps using the BP-300 potentiostat, imitating a two-electrode system. As no changes were noticed, a few other setups were tried as well, including sandwiching a hydrogel layer between two custom pre-available

carbon textile electrodes and using a blob of the gel to connect the two sides of a gold-covered ion-permeable membrane.

3.1.6 Detecting the movement of cations in carrageenan hydrogels

According to the presumption of the reversibility of carrageenan gelation, such a process would include dissociation of double-helical aggregations, followed by a release of the cations binding them and the subsequent movement of the latter to the anode through the electrolyte-containing matrix. Thus, an attempt to gain proof of such elasticity changes by detecting movement of metallic cations was made by performing CV measurements on salt-cured κ-carrageenan hydrogels. A Micrux (Spain) ED-SE1-Au microfluidic chip with titanium/gold electrodes on a glass substrate was utilized to that end[94]. All the measurements were performed using the BP-300 potentiostat in a three-electrode configuration. The measurements were performed both on the hydrogel samples and blank salt solutions for comparison; glycerol was added to prevent the sample drying over long measurements. Finally, the $CaCl_2$ solution was replaced with a 0.45M K_2SO_4 one to obstruct the potential reaction of gold with chlorine.

3.1.7 SEM and EDX study of carrageenan-carbon composites

In order to get some understanding of the structure of the created composites and to gain an overview of the devised methods' feasibility, microscopy of a small sample of the dried composite film was performed. Images of both the film's surface and the cross-section, the latter obtained by freezing a piece of the sample and breaking it in half, were gained through SEM using a Hitachi (Japan) TM3000 electron microscope. Additionally, EDX spectroscopy study was done to see the distribution of the components in the composite using the built-in detector of the microscope.

3.1.8 Checking the conductivity of the composite by modifying CF surface

To obtain data on the conductivity of carrageenan-carbon composites, a setup was made using a 3D printed electrochemical cell. First tests were run on a strip cut from the same dried sample that was used in the SEM/EDX tests.

Cyclic voltammetry was performed in a 5 mM solution of ferro/ferricyanide in 7.4 pH PB, with an Ag/AgCl reference and CFMB counter electrodes. The select potential window was -1 to +1 V and the scan rate was 20 mV/s. Unfortunately, the film was found to have very poor conductivity and showed very intensive swelling (which made the sample too big to fit into the printed cell altogether). The discussion and considerations that followed led to a suggestion that

the contact area of the sample and the connection clamp might have been insufficient, which led to the design of a new setup.

CFMB electrodes (working and the counter) were prepared by cutting the bundles of required length and closing the capillary flow using nail polish. Using a printed cell of a similar design, CV measurements with the same parameters were then performed first in a 7.4 pH PB and then in a 5 mM ferro/ferricyanide solution in the same buffer. Then, the lower part of the CFMB working electrode was covered in a carbon/carrageenan ink mixture and the measurements in the 5 mM ferro/ferry solution were repeated. Parallel to the voltammetry, EIS measurements were performed for each step (on the 10 mV potential with the frequency varying from 100 to 0.1 kHz).

3.2 RESULTS AND DISCUSSION

3.2.1 Optimisation of 3D printed electrochemical cell and electrode design

The design of the electrochemical cell consisted of a 3D printed cap which was designed (using Solidworks software) to fit 6 analysed units of CFMB electrodes at once. The cell had a diameter of 26 mm with 6 channels of 3 mm diameter and 44 mm length each (made to prevent the contact and interaction between the working electrodes). 2 more cavities with a 6 mm diameter were purposed to fit reference and counter electrodes. In the printing process, a 0.4 mm nozzle was utilized for shaping flexible filament material, the latter selected due to its elasticity and resistance to deformation. The printing was performed in 240 Celsius extrusion temperature while the temperature of the bed was 50 Celsius. The printing speed of 20 mm/s was deemed to be optimal with a 0.2 mm slice taking a total printing time of 1 h 57 min. The rendered image of the electrochemical cell (***Fig. 9***) is included to indicate the suitability of general lab glassware to house the cap.

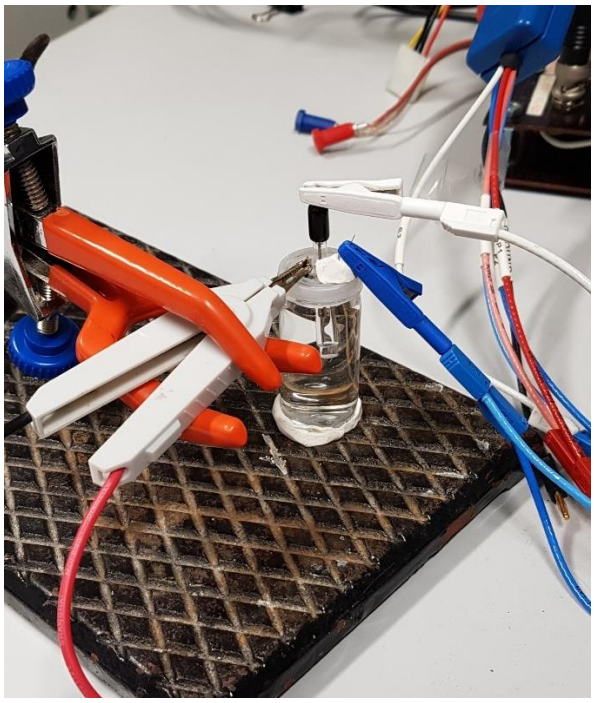

Figure 8. *A photo of the prototype of the proposed design. It was produced by drilling holes in the cap of a commercially available vial. Small sizes of the holes and general lightness made it unstable which had to be fixed by market-obtained sticker paste.*

Figure 9. *The design of electrochemical cells used for CFMB electrodes.*

The CFMB electrodes were placed into the designed printed cap to combat the fibre microunit fragility, increase the reproducibility of their length and reduce the influence of its variation on the electrochemical response as well as to prevent the contact between the multiple samples.

For the fabrication of the CFMB electrodes, bunches of about 600 fibre units were taken and to cut desired lengths. The capillary flow was prevented by depositing a drop of nail polish (nitrocellulose in a mixture of organic solvents) at some distance from the edge to form a hydrophobic barrier, additionally serving as the binder for the bundle. The electrical connection was realized at the far end of the bundle, separated from the working area by the nail polish barrier.

The electrodes were then inserted in the 3D printed cap and dipped into the electrolyte, the design allowing to keep the electrode area constant with a fixed length of 2 cm. Two considerations of the electrode area are presented further on.

3.2.2 Characterisation of carbon electrodes using microscopy

SEM analysis of a CFMB electrode was performed after freezing the sample in liquid nitrogen and cutting it using a scalpel (***Fig. 10***).

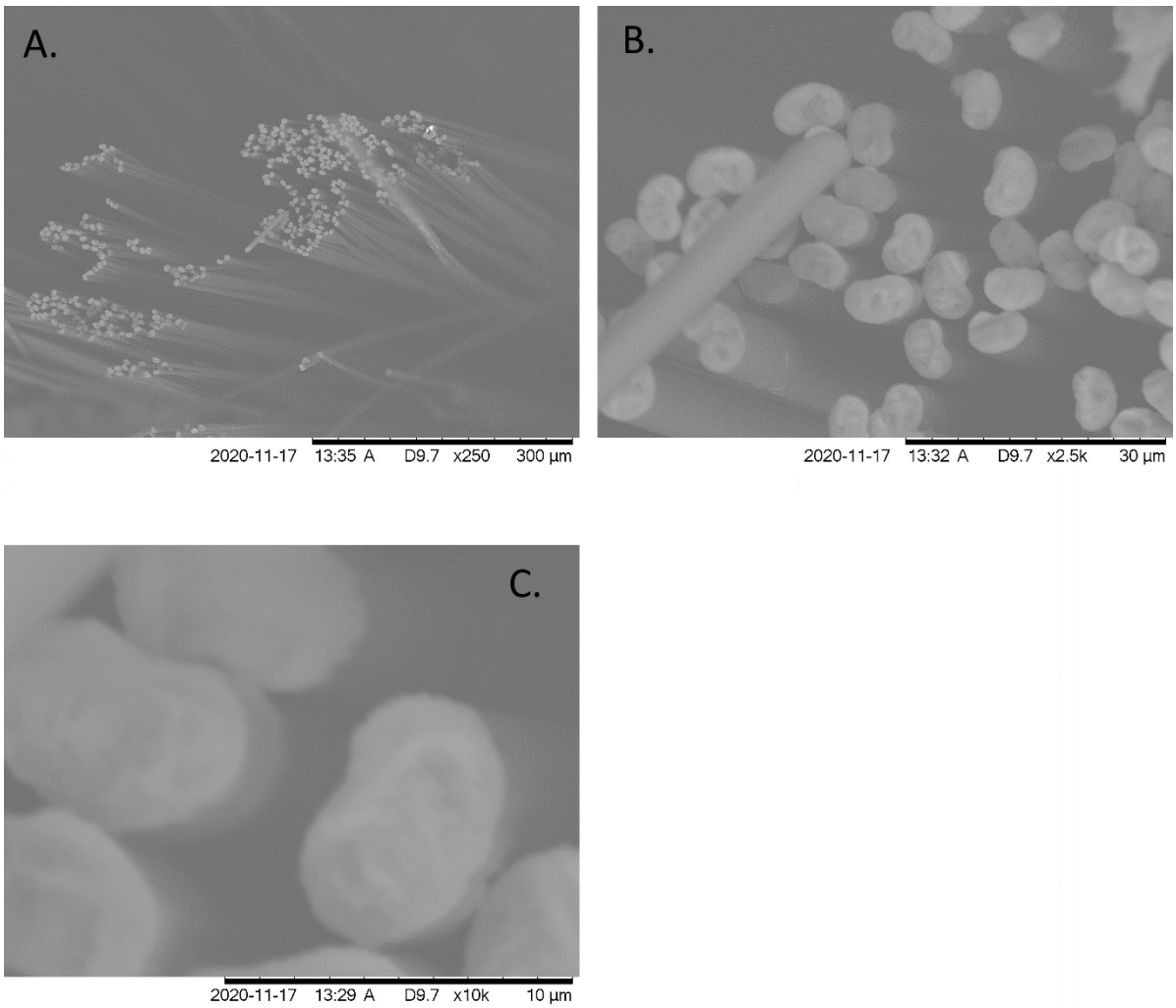

Figure 10. *The pictures of the cut CFMB electrode, obtained at 250x, 2500x and 10000x magnifications.*

The number (N) of microcylinders was derived from the mass of the CFMB electrode using the formula $N = m/(r^2 L_0)$, where *m* is the microbundle mass (7 x 10^{-3} g), *r* is the radius of a single microcylinder unit and L_0 is the total length of the electrode (12 cm). The gained value of N was 843 microcylinders. Two notions of a geometrical CFMB area were then considered.

If the wet bundle is placed in the air, the fibres are packed tightly, and the bundle can be presented as a single cylinder with its outer side being the geometrical area of the electrode. The area (A_{bulk}) can then be calculated as follows: $A_{bulk} = r^2 N(1 + 2L/r)$, with the gained area value turning out to be negligible (A_{bulk} = *0.008* cm^2).

If the fibre units are placed in water or electrolyte, the fibers bend at some angle and cause a higher area to be exposed to the electrolyte. The geometrical surface area of the CFMB in water (A) can then be calculated through the sum of independent areas of each microcylinder unit using the following equation: $A = 2mL/(rL_0)$, where L_0 is the total length of the CFMB electrode and L is the length of the electrode part that is immersed in the electrolyte. The

calculated geometrical surface area value of the CFMB was 3.721 ± 0.025 cm^2 and was used further on to normalize gained electrochemical signals and in calculations of diffusion coefficients.

3.2.3 Electrochemical characterisation of carbon electrode in neutral phosphate buffer

Phosphate buffer is the most frequently used buffer for electrochemical sensing experiments that require a neutral pH. To characterize the CFMB electrodes, blank CV scans were performed in 7.4 pH PB were done at various scan rates (10, 20, 50, 100, 200 and 400 mV/s). At the voltage of -761 mV a massive reduction peak appeared, related to the oxygen reduction of the oxi-species (phenolic, hydroxyl and carboxylic groups) on the carbon electrode, which may be attributed to these major functional groups being present during the manufacturing process of the carbon fiber. Compared with peak potentials for oxygen reduction in a screen-printed electrode (-629 mV) or screen-printed graphene nanoplate electrode coated with a phytic acid-doped polyaniline film (approximately -600 mV)[95] in the same 7.4 pH PB, CFMB electrode oxygen reduction has a significantly more negative peak potential (-764 mV), making it a good candidate for applications requiring wider potential windows, close to graphene-modified screen-printed carbon and (-806 mV) in 50 mM 7.2 pH PBS[96].

An unknown reversible redox process was present between -200 and +500 mV, with an initial potential of +14 mV. It can be noted that when the potential window was made narrower (300 to +800 mV), no redox reaction was observed, making it possible that the presence of oxygen excited the molecules. Peak-to-peak separation was relatively small ($E_p = 153\ mV$ at 10 mV/s), suggesting a low resistance for the electron transfer between the oxygenated groups and the fibers. EIS data indicated resistor-like behaviour of CFMBs at higher frequencies (with electrolyte resistance being 68.4 Ohm), with a straight line attributed to capacitive systems appearing at the lower frequencies (10 kHz). It can be suggested that the surface of the microbundle and the electroactive species physically adsorbed to the oxygenated groups at the fiber surface serve as a capacitor together.

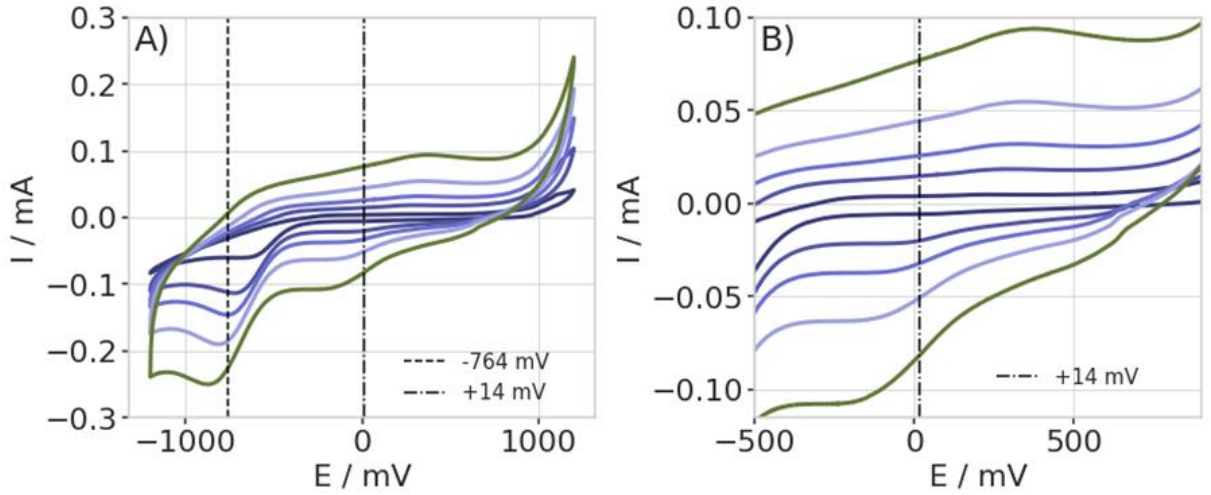

Figure 11. A. *Voltammograms of the CFMB electrode in 0.1 M PB (pH 7.4) measured vs. Ag/AgCl and 14 mV OCP voltage at various scan rates (10, 50, 100, 200, 400 mV/s) in a -1200 to 1200 mV potential window* ***B.*** *Zoom in on the CVs' area to see the redox species on the surface of the CFMB electrode;*

Another way to provide information about such surface-confined redox species could be Cole-Cole plots of imaginary capacitance (pseudocapacitance/redox reactions, C'') vs real capacitance (C'). Real and imaginary capacitances are given by $C' = -Z' \frac{1}{2\pi f Z}$ and $C'' = -Z'' \frac{1}{2\pi f Z}$, respectively, with Z' and Z'' being the real and imaginary impedance components and f is the frequency. From this analysis, the small wave seen at the CVs at 14 mV can be attributed to pseudocapacitive charging of a redox-active layer on the CFMB surface, with capacity of 48 μF.

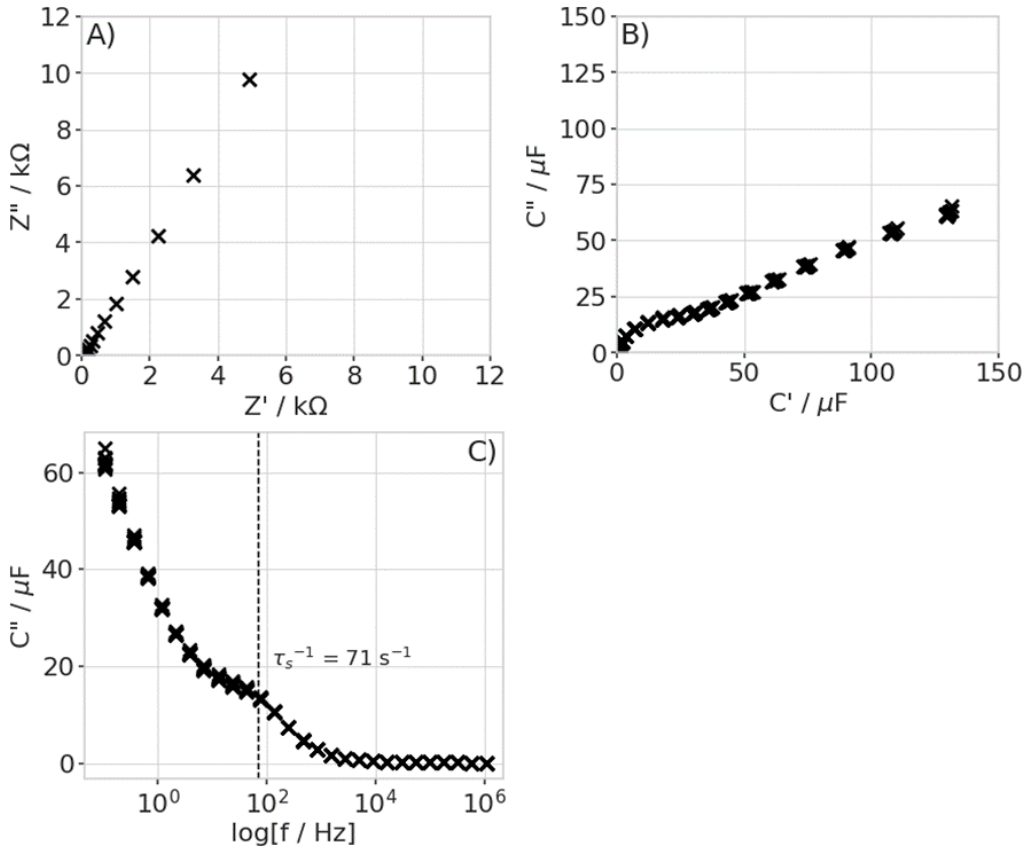

Figure 12. A. *Nyquist plot of CFMB in 0.1 M PB measured on frequencies from 1000 to 0.1 Hz, amplitude of 10 mV at OCP (14 mV), illustrating the position of R_s in 0.1 M PB, originating from CFMB electrode impurities (1,2-naphthoquinone).* ***B.*** *The Cole-Cole plots illustrating the pseudo-redox capacitance of the porous redox-active layer* ***C.*** *Plots of C'' versus frequency illustrating the location of the time constant.*

The plot (***Fig. 12 C***) allowed for derivation of the relaxation (RC) time constant (τ^{-1}), found to be 71 s^{-1}, somewhat consistent with previous data for other impurities on a bare screen-printed electrode (τ^{-1} = 242 s^{-1}).

This redox behavior of CFMB can be suggested to happen due to presence of redox molecules (e.g., presumably, 1,2-naphthoquinone) on its surface as an impurity leftover from the epoxide resin binder manufacturing process, where quinone is incorporated to improve the mechanical properties of the produced fiber. Naphthoquinone is also present as an ink-binding compound in screen-printed electrodes available commercially.

3.2.4 Electrochemical characterisation of carbon electrode in redox probe

Ferrocene is the primary redox species sample used to analyse electrochemical sensors and gain information on electron transfers. So, EIS measurements in 2.5 mM $[Fe(CN)^6]^{3-/4-}$ prepared in

7.4 pH PB were performed. A slightly higher solution resistance value than in pure PB was observed with OCP voltage of 197 mV at the frequency of 50549.29 Hz. Observations of load transfer resistance (R_{ct}), which serves as the primary Faradaic impedance characterisation character, were done at low frequencies (1.97 Hz), and a value of 101.403 was gained (it represents the diameter of the semicircle on the low-frequency part of Nyquist plot, Randles equivalent circuit).

Effects of the changes of the scanning rate were then studied using 0.5 mM solution of ferro-/ferricyanide in the neutral pH buffer (***Fig. 13***). For each scan rate, the average ratio of anodic (I_{pa}) to cathodic (I_{pc}) currents was 1 and peak currents, just like the peak potentials, increased linearly with the square root of the scan rate. The observed peak separation value (E_p) was 610 mV at 100 mV/s scan rate, significantly more than the value of 57 mV for an ideally-reversible redox pair, and the value of E_p also increased with the scan rate, similar to previously reported peak separation for Au and Pt nanoparticle-modified screen-printed carbon electrodes (157 mV for 5mM ferro/ferricyanide pair in 0.1 M 7.4 pH PBS)[97], or graphene-modified screen-printed carbon, both clean (0.273 V), modified with triangle ruthenium nanoparticles (0.308 V) or with an o-Phenylenediamine film (0.181 V) (0.5 mM ferrocyanide in 50 mM 7.2 pH PBS)[96]. Altogether, this indicates near-reversibility of the pair with it being influenced by heterogeneous electron transfer dynamics and controlled by semi-infinite linear diffusion. The gained EIS results served as the confirmation of this with 45-degree straight upwards line present on the Nyquist plot lower frequency area, indicating a diffusion-limiting process.

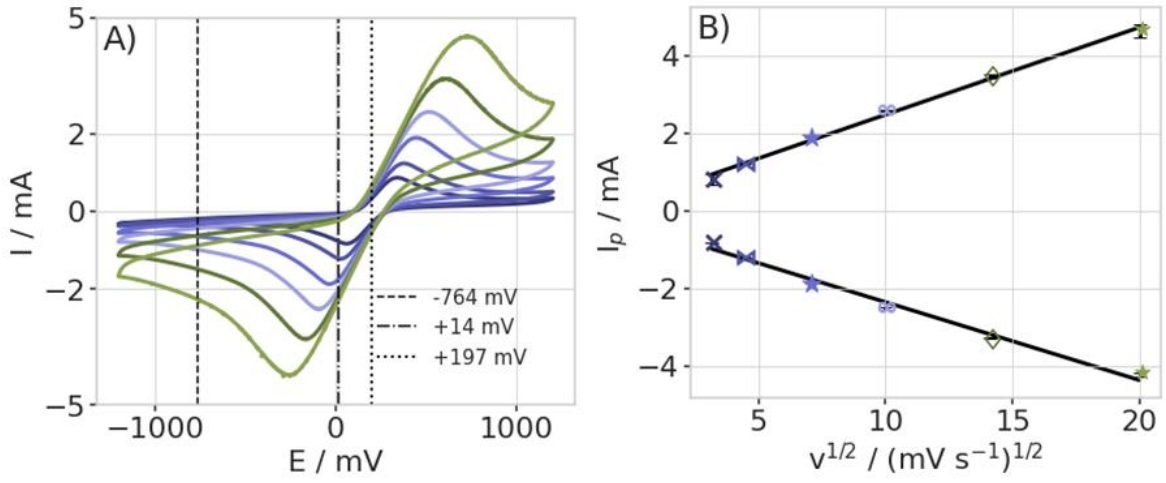

Figure 13. *A.* *CV of CFMB electrode in 2.5 mM of [Fe(CN)6]3-/4-, supported by 0.1 M PB, from -1.2 V to 1.2 V vs. Ag/AgCl, at different scan rates (10, 20, 50, 100, 200, 400 mVs^{-1}),* ***B.*** *the dependence of the peak current on the square root of the scan rate.*

The diffusion coefficient (D_0) was derived from the analysis of the peak currents (I_p) obtained at several scan rates and performed according to Randles-Ševchik equation: $D_0 =$

$k\frac{2RT}{0.217A_2C_2n_3F_3}$, where k is the slope or $\frac{I_p}{vA}(V/s)^{-0.5}$, n is the overall number of electrons in the electrochemical reaction (in this case, *n = 1*), F is Faraday constant (96485 C/mol), C is electroactive species concentration (2.6 x 10^{-6} mol/cm^3), A is the geometrical surface area of the electrode (~3.7 cm^2), v is the scan rate, R is gas constant (8.3145 J/(K×mol)) and T is temperature (293 K). The slope values derived using the obtained I_{pa} and I_{pc} were -6.36 x 10^{-3} ± 0.032 x 10^{-3} $A(V/s)^{-0.5}$ and 7.12 x 10^{-3} ± 0.44 x 10^{-3} $A(V/s)^{-0.5}$. Using the average of their slopes, then, D_0 calculation was performed with a resulting value of 6.66 ± 1.02 x 10^{-6} cm^2/s, which is comparable to previously provided diffusion coefficients for ferrocene investigated on screen-printed electrode sensors.

3.2.5 Stability and reproducibility of carbon fibre bundle electrodes

It is quite important for an electrochemical cell to be reproducible, as it allows to eliminate the need for electrode calibration in prior. To check the reproducibility of the considered design, variability of the produced CFMB electrode length influence on electrochemical activity was studied, with CVs of 6 different CF electrodes being performed in 7.4 pH PB (***Fig. 14***).

Figure 14. *A photo of set-up 3D printed cell before the CV stability tests.*

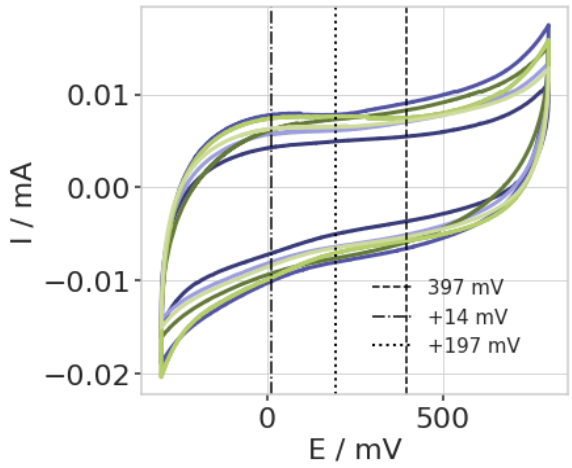

Figure 15. *CVs done in 0.1 M PB at 100 mVs-1, graphs from 6 different CFMB electrodes in a 3D printed electrochemical cell.*

Fig. 15 shows CVs of different electrodes with background current variation being less than 10%. To check electrode stability, three cycles of 2.5 mM $[Fe(CN)_6]^{3-/4-}$ in 7.4 pH PB at a scan rate of 100 mV/s were recorded on each electrode. Throughout all the cycles the E_{pc} and E_{pa} values for a single electrode remained constant. I_{pc} and I_{pa}, too, showed little variation. The measurement errors within the electrode for the peak currents were 0.38% and 1.12% for I_{pc} and I_{pa}, respectively, while between electrodes the errors were 5.04% and 6.07% for cathodic and anodic peak currents. All this data serves to demonstrate good stability and quite small measurement errors.

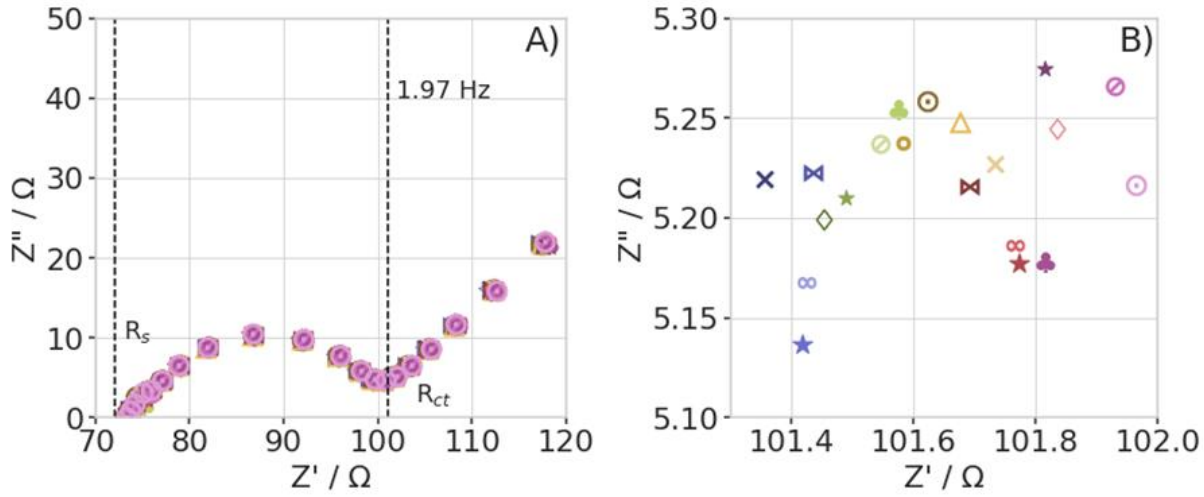

Figure 16. A. *EIS Nyquist plots of CFMB electrode in 2.5 mM ferro-/ferricyanide solution in 0.1 M PB, at OCP voltage (197 mV), with R_{ct} being possible to extract from the semicircular region of the run spanning the frequencies from 100000 to 0.1 Hz.* ***B.*** *The zoom-in on the R_{ct} zone located at 1.97 Hz. Various markers serve to indicate the measure of the system's stability (across 20 tests);*

In a stability test, EIS revealed minor change in R_{ct} values (at f = 1.97 Hz), which stayed within 0.29 percent over 20 scans, being consistent with CV cycling stability, 0.38 percent from I_{pc}.

3.2.6 Testing of carbon fibre bundle electrodes for sensing of dopamine

Dopamine (DA) is a neurotransmitter, a compound serving to relay nerve impulses. It is associated with the feeling of happiness and the process of learning in humans, as well as activities of cardiac and nervous systems, regulation of body weight and can serve as a biomarker for some diseases.

The produced CFMB electrodes were tested for DA electrochemical detection in 7.4 pH environment (selected due to its closeness to human body conditions) created using 0.1 M PB; to that end, CV was performed on an unmodified CFMB electrode. During the blank zero-dopamine scan no clear redox reaction was seen in the potential window from -300 mV to 800 mV, chosen purposefully to evade oxygen evolution.

After 10 M of DA was added into the cell, a small wave appeared on the voltammogram both in the oxidation and reduction regions, indicating the expected one-electron oxidation of DA. The location of the oxidation peak was at +397 mV, demonstrating higher effectivity than screen-printed electrodes in comparison with the literature-available data. E_0 value for DA is the same as in some other redox species, showing potential for DA oxidation catalysis. In fact, the quinone seemingly present in the outer layer of the fibers can promote electron transfer reactions and, as a result, reversible electrochemical response with significant long-term effects on DA oxidation.

The I_{pc} values for the range of DA concentrations between 10 and 100 μM were extracted from the gained voltammograms. As became evident from their analysis, their dependence on DA concentration was linear. To perform normalization of the peak currents at select concentrations, the following formula was used: $RR\%\ (\%) = \frac{I_{target} - I_{blank}}{100 I_{blank}}$, where I_{target} was the I_{pc} at the select concentration and I_{blank} was the current value at 0 M DA[98]. At 100 μM DA RR value reached 600% and sensitivity, extracted from the calibration slope's curve, was 428 nAM. Normalization of the sensitivity was then performed, as it is usual, to the area of the electrode. Using the two previously considered methods for surface calculation of CFMBs two values of normalized sensitivity were gained: sensitivity of a packed electrode (with A_{bulk} = 0.008 cm^2) reached 53.5 A/(M x cm^2) and sensitivity of the fully unpacked form reached 115.67 nA/(M x cm^2). Such a sensitivity is comparable in magnitude to screen-printed (200 nA/(M x cm^2)), 2D pyrolytic carbon (372 nA/(M x cm^2)) and pyrolytic carbon nanograss (773 nA/(M x

cm^2)) electrodes to DA. Higher sensitivity values could potentially be achieved by increasing electrode roughness or porosity.

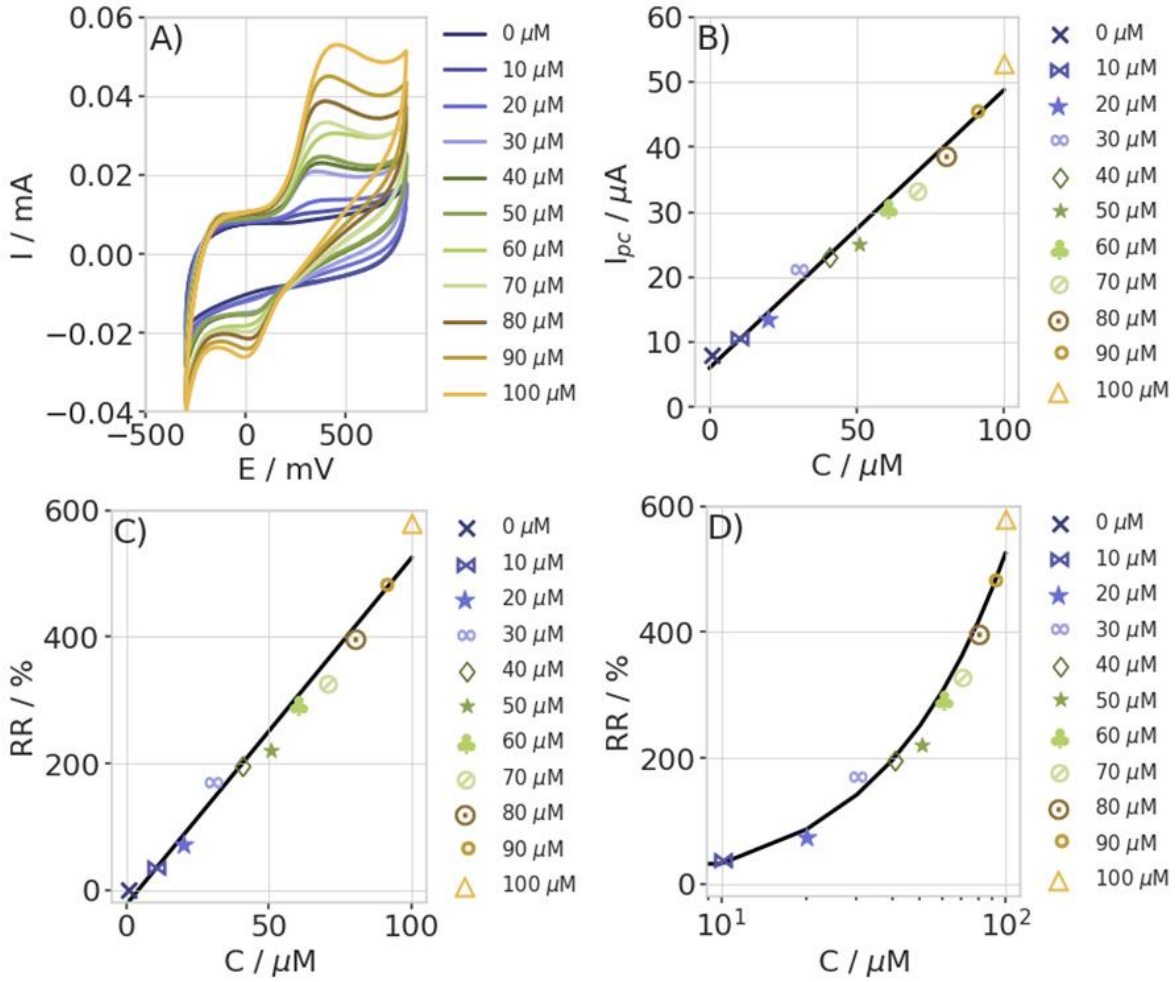

Figure 17. *Detection of DA with a CFMB electrode in 0.1 M 7.4 pH PB. Potential window of CVs was -300 to +800 mV, measurements were done vs Ag/AgCl.* ***A.*** *CVs for the blank scan and with DA added in 10 µM steps up to 100 µM total concentrations. The scan rate was 100 mV/s.* ***B****. The calibration curve obtained from the CVs; I_{pc} values plotted versus the DA concentration.* ***C****. The calibration curve normalized to the blank solution current (R^2 value was 0.978).* ***D****. The calibration curve with the logarithmic axis used for concentration.*

Because the area of electrodes is usually taken into account, the limit of detection (LOD) may be a better parameter to use when comparing sensitivities between platforms. As a result, the DA's LOD was calculated using the formula $LOD = \frac{3\sigma}{slope}$ where σ is the standard deviation for the y-intercept of the calibration curve plot, just as for the various non-modified electrodes used in previous research for measuring[98,99]. The gained DA value was 8.85 µM. Similar values were obtained on a screen-printed electrode (LOD = 4.8 µM) in the literature. Also, the various

modified electrodes had LOD of the same order of magnitude, for example, reduced graphene oxide modified GCE had LOD of 6 μM and aspartic acid grafted GCE had LOD of 1.2 μM. Despite the ease of using CFMB electrodes integrated in a 3D printed cell for electrochemical purposes, the ability to achieve relevant results for DA detection was demonstrated, once again without any electrode modification or treatment.

3.2.7 Reversible gelation

It was at first suggested that the reversion of the elasticity change could be visible with a naked eye and possibly lead to a slight noticeable movement on its own when subjected to electricity. The expected response of cation-induced gelation was indeed achieved and served as the basis for the creation of coatings and self-standing films produced during the work. During the experiments it was found out that for the physical stability of the coatings and the films water-carrageenan mixes of approximately 1% to 2% were sufficient as the basis. Mixes of higher concentrations were assuming a gel-like state on their own in room temperature, requiring melting before shaping could occur. Overly high concentrations (~10% w/w or even smaller) led to complications during the preparation of the polymer solutions, namely, incomplete dissolution of the carrageenan powder due to what seemed like wet powder clustering together and forming a gel coating on the outer layer. Such clumps proved to be quite stable and invulnerable to both temperature and physical influence of the stirring bead and required to be manually destroyed using a spatula or a similar tool, with 10% w/w carrageenan mixes forming a whole layer of the wettened powder which proved to be impossible to disperse even manually. The most used binder in the composites produced during this work was thus a 1% w/w carrageenan/water solution.

To check this suggestion, a simple experiment was set up: two strands of woven carbon fibre fabric were glued together by successively dipping the end of each strand into pre-made κ-carrageenan/water mixture of approximately 1% (w/w) and 0.5M solution of $CaCl_2$. The ends of the strands were then connected and allowed to bind with the thickening gel blob (with the already connected part of the strands being dipped into the salt solution one more time together). The fibres were then connected to the potentiostat and subjected to a triangle-wave potential sweep, imitating a two-electrode system in an ionogel electrolyte. The used scan rate was 50 mV/s and the selected potential window was from +1 to -1 V. Sadly, no visible change was noted, presumed at the time to be due to insufficient conductivity of the fibres.

A similar experiment was then done using custom carbon textile electrodes (made of the same woven carbon threads used before) with AgCl paste connections isolated with silica glue. Like

in the previous setup, the electrodes were glued together using the $CaCl_2$-cured κ-carrageenan, this time deposited in layers using a brush (the first electrode was covered with a layer of carrageenan followed by chloride, finally covered by the second electrode already having an identical carrageenan layer). The potential sweep settings used were the same as in the previous setup. Once again, no visible changes occurred, and an attempt was made to increase the conductivity of the hydrogel by submerging the electrodes in the chloride solution. Still, no changes were seen, and the electrodes were left to soak overnight with a hope that diffusion of the salt into the sample with time will lead to changes. Unfortunately, it also led to the dissolution of the AgCl paste due to improper Si glue coverage.

Another setup was then devised to see any visual changes of carrageenan hydrogel sample. A gold-covered ion-permeable membrane was dipped into the $CaCl_2$ solution, then dipped into the carrageenan mixture followed by another submersion into the solution of chloride. The membrane was then connected to the potentiostat from both sides and subjected to the same triangular wave potential sweep. As no effects were seen with a naked eye, attempts were planned to observe the sample under a microscope during a sweep, however, the setup designs were complicated by the shape and size of the available connection clamps. Additionally, an observation was made that care should be taken while using $CaCl_2$ for curing the hydrogel samples, as the swelled gels contained a significant amount of Cl^- ions able to react with the gold on the membrane, made evident by a patch that appeared on one after some usage. A decision was thus made to replace the $CaCl_2$ with K_2SO_4 in the experiments to come, as K^+ ions were also known as gelating agents for the carrageenan and the sulphate is quite inert with regards to gold.

To simplify the observation of the gel sample and improve the setup, a Micrux ED-SE1-Au microfluidic chip with titanium/gold electrodes on a glass substrate was used. As the available connector/holder was overly large, it would make placement of the chip under the microscope impossible, thus the chip's contacts were soldered to tin-plated copper cables to provide connection (***Fig. 18***).

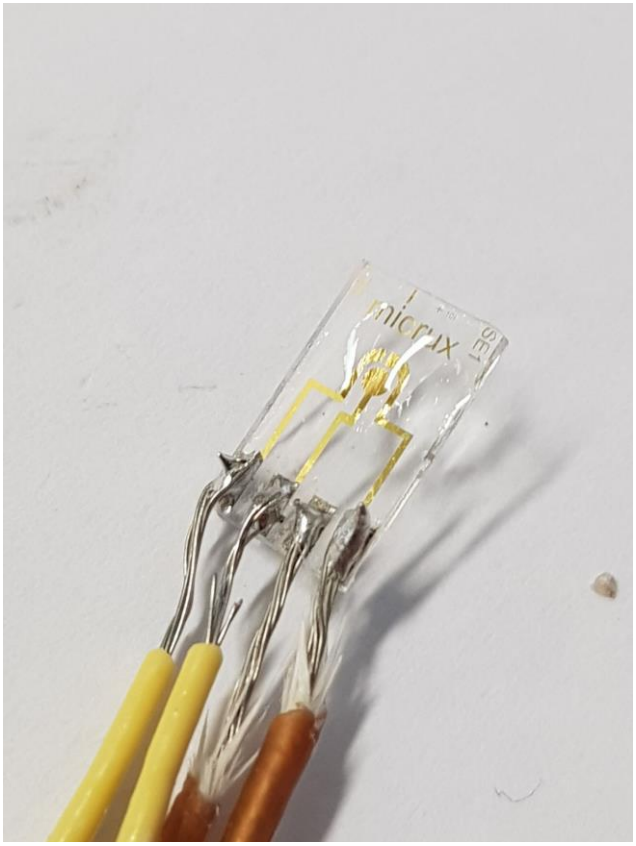

Figure 18. *The microfluidic chip used in the experiments with the tin-plated copper wires soldered to its contacts. A salt-cured carrageenan sample can be seen deposited onto the chip's working area.*

The samples were prepared by depositing a drop of κ-carrageenan onto the working area of the chip with a brush, the latter then washed with milli-ρ water and used to deposit 0.45M K_2SO_4 on top of the jelly, smearing it slightly. Cyclic voltammetry was then performed on 10 mV/s scan rate in the -0.85 to 0.85 V scanning window (the potential interval was decreased to evade water electrolysis). After multiple cycles of the voltammetry testing visible changes were noticed, and the experiment was redone with the sample placed under a microscope. The resulting changes were found to be caused by the drying of the sample gel (***Fig. 20***).

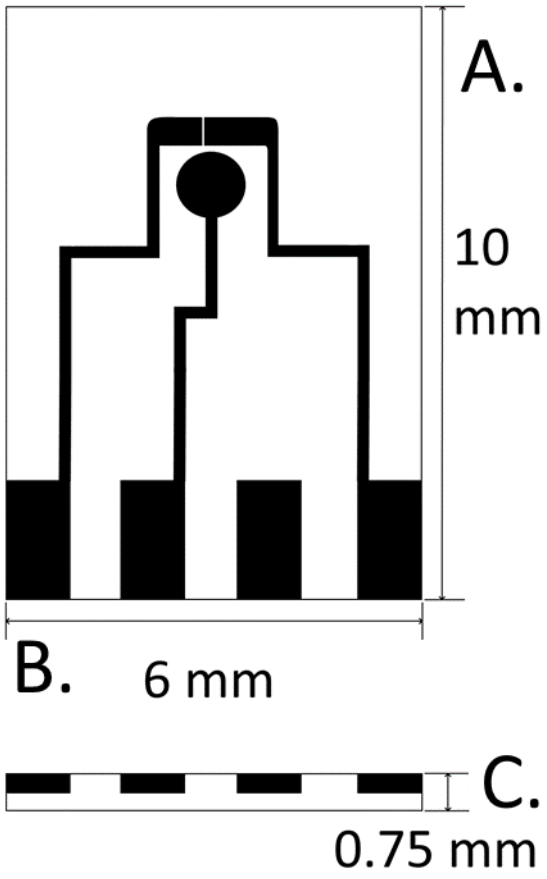

Figure 19. *The dimensions of the microchip used:* ***A.*** *length,* ***B.*** *width and* ***C.*** *thickness. The diameter of the WE is 1 mm.*

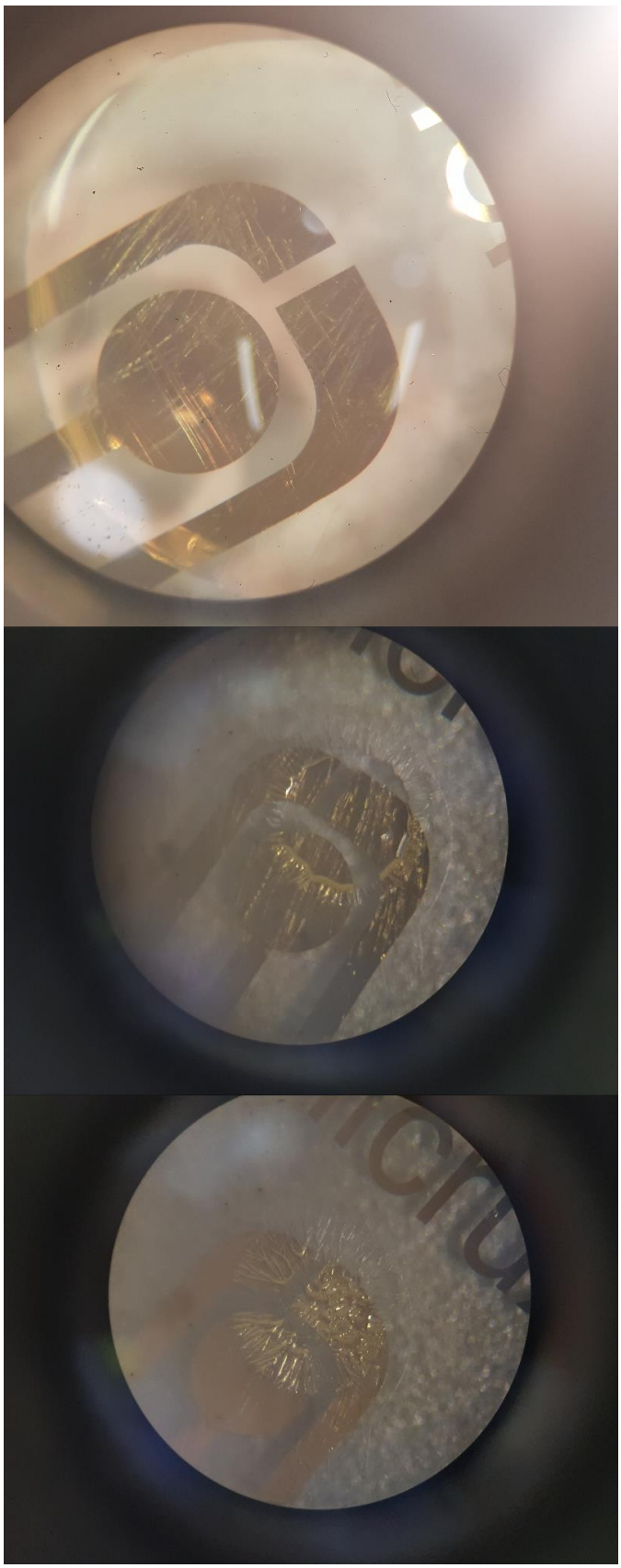

Figure 20. *Pictures of carrageenan hydrogel samples on the microfluidic chip, taken on various stages of a cyclic voltammetry run. Drying of the sample can be seen as it is subjected to current.* ***Top to bottom:*** *a fresh sample of hydrogel, the sample some time into the run, the sample by the end of the*

voltammetry. All pictures were taken using an optical microscope under the room-condition illumination.

To prevent the drying, glycerol was used to cover the whole sample. The fluidity of glycerol, however, led to at least partial mixing with the gel and introduced additional interference (***Fig. 20***). To compare the results, blank scans of a glycerol-sulphate mix were taken, too (***Fig. 21***).

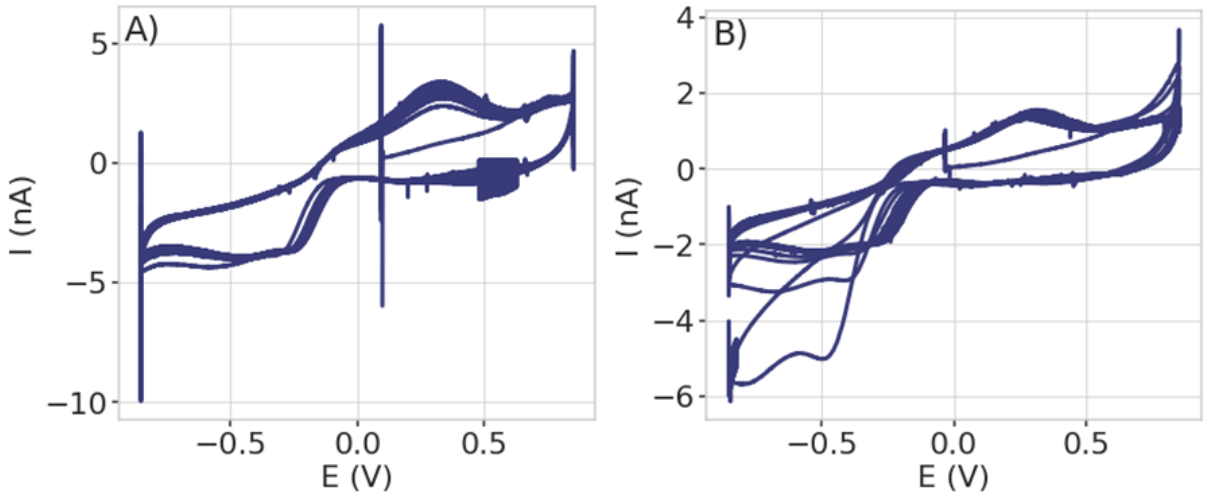

Figure 21. *Cyclic voltammograms for K_2SO_4-cured κ-carrageenan hydrogel without (**A**) and with (**B**) glycerol deposited on top; the analysis was performed in -0.85 to +0.85V potential window for 10 cycles on a 10 mV/s rate (the spikes noise is coming from the contact area). For each voltammetry, 11 cycles were performed including the initial one.*

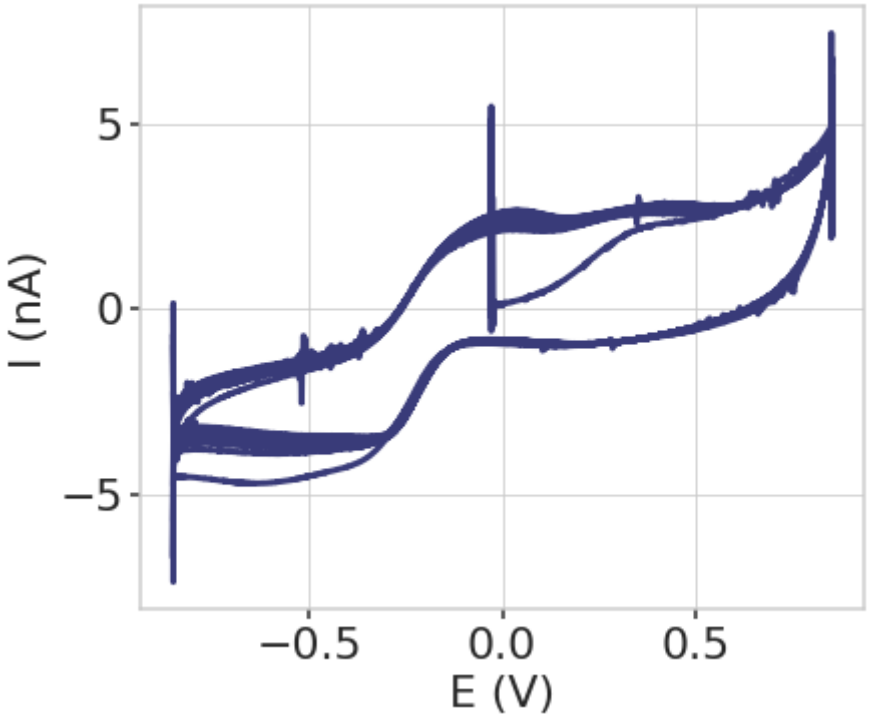

Figure 22. *The cyclic voltammogram for a drop of K_2SO_4 mixed with glycerol. The voltammetry settings used and the number of cycles done were the same as for the samples containing carrageenan (the spikes noise is coming from the contact area).*

Peak analysis was then performed for the 10th cycle of each gained voltammogram, with peak potentials, currents and peak-to-peak separations being found, as well as calculations being done to derive half-wave potentials (***Table. 1***).

Table 1. *Peak potentials, currents and half-wave potentials for the performed CVs.*

	E_{pa}, V	E_{pc}, V	i_{pa}, nA	i_{pc}, nA	E_p, V	$E_{1/2}$, V
K_2SO_4-cured carrageenan	0.319	-0.2488	12.51	13.15	0.5678	0.0351
K_2SO_4-cured carrageenan with glycerol	0.301	-0.238	4.99	7.67	0.539	0.0315
K_2SO_4 in glycerol	0.04938	-0.2967	1.564	14.69	0.34608	-0.17304

As evident from the CVs, there were no peaks to assume any specific movement of cations possibly attributed to some unforming of the carrageenan helical aggregations under voltage.

The movement of ions in the sample can seemingly be connected to the movement of ions in the residual salt solution that the hydrogel is swollen with.

Altogether, the reversion of the cation-induced gelation of κ-carrageenan was not achieved during the experiments. The hydrogels of carrageenan cured using positive metal ions did not show any changes in elasticity significant enough under the influence of high-rate triangle wave potential sweeps, while the slower rates inevitably led to drying of the hydrogels and made it impossible to check the visible elasticity change. Attempts to prove the possibility of some reversion occurring through the form of movement of metal cations in the carrageenan gel samples produced results indicating lack of any ionic movement that could not have been attributed to the movement of the ions of the salt solution slowed by the matrix of the gel.

3.2.8 Carrageenan composites

Both self-standing film composites of activated carbon and κ-carrageenan and composite film coatings were produced during the work. The mixing process was improved through multiple attempts and the resulting procedure (***Fig. 24***) allowed for simple, direct production of the films using only biocompatible reagents. The created samples were characterized using the SEM and EDX methods, both on the surface and the cross-sections of the produced films. Electrochemical tests, CV and EIS, were performed to estimate the conductivity and ion permeability of the composite material. The dried composites were found to swell when submerged in liquid for some time, so attempts to test the extent of swelling were made, but mostly failed due to crumbling of the samples.

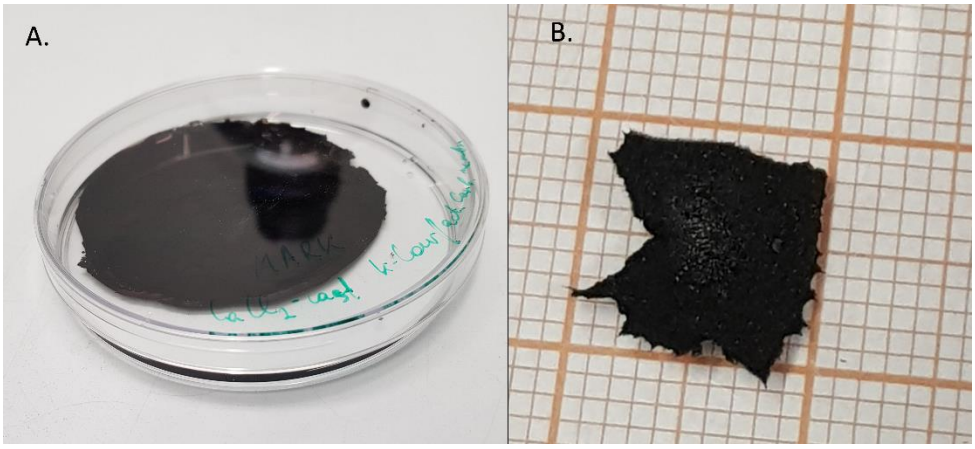

Figure 23. ***A***. *One of the composite films made during the work, plated and stored in a Petri dish. This sample was used in the microscopy studies of film cross-sections.* ***B.*** *A piece of the first film sample made during the work. The sample was dried to prepare it for microscopy; the piece present here was then subjected to swelling in 7.4 pH PB buffer in an attempt to test the swelling and then dried again. The edges are noticeably uneven and the piece seems to be shrunk due to surface tension-like effects.*

Based on the already known and used structure for supercapacitive laminate soft robots[22], a design was devised (***Fig. 25***) for a variable-elasticity carrageenan-based actuator. Similar to the conventional EDLC-like soft robot, the design consisted of two electrodes separated by an ion-permeable material and a layer of ionogel and covered with gold film current collectors on both sides.

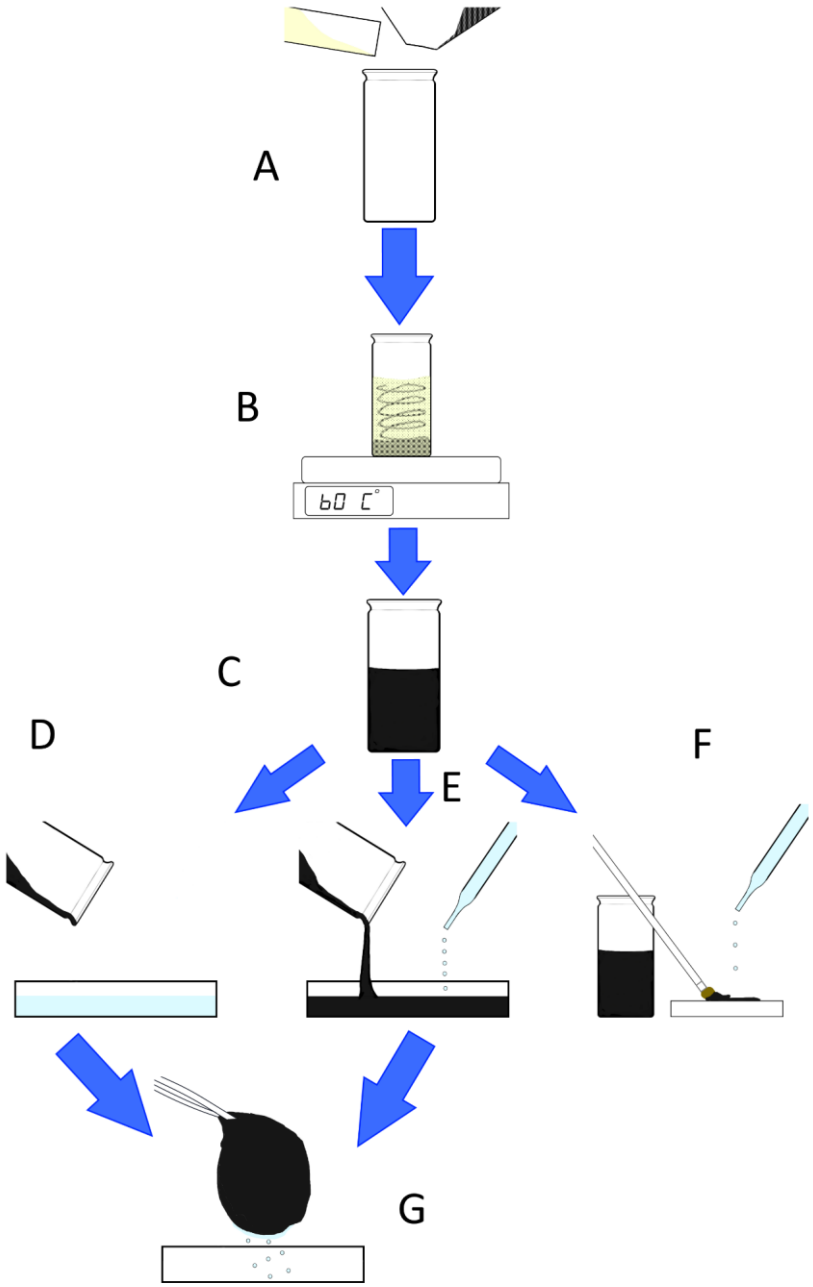

Figure 24. *The process of the making of the carrageenan/carbon composition.* ***A****. The measured weighed amounts of the carrageenan/water mixture and the activated carbon powder are added into a vessel.* ***B****. The mix is heated at 60 Celsius and continuously stirred with a magnetic bead overnight.* ***C****. The produced suspension of carbon in carrageenan.* ***D****. One of possible casting methods: the suspension is poured into a mould already containing some amount of the salt solution.* ***E****. Another casting method.*

*The suspension is poured into the mould and covered with the salt solution using a dropper. **F**. The method used for making coatings. The suspension is deposited onto the target substrate using a brush, and the resulting cover is then coated with the salt solution using a dropper. Alternative curing methods may include the dipping of the substrate into the salt solution or deposition of the latter using a brush, though their applicability depends on the form of the substance and required precision. **G**. The slab of the solution-swelled hydrogel-carbon composite produced as a result of casting.*

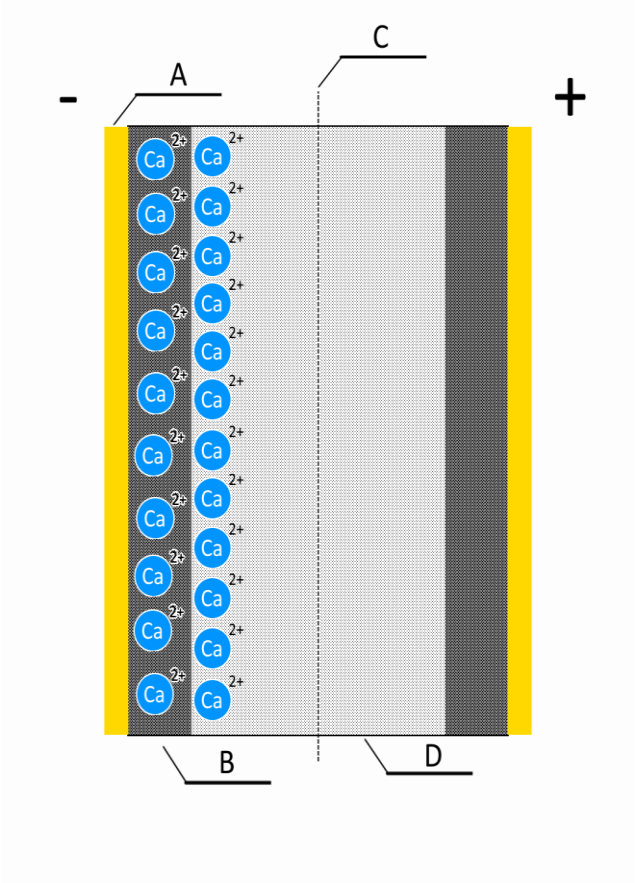

***Figure 25.** A schematic of the proposed soft robot design. **A.** Gold film current collectors. **B.** Carbon/carrageenan composite electrodes. **C.** Ion-permeable membrane serving to prevent the short-circuiting of the EDLC. **D.** A layer of carrageenan hydrogel serving as an ionogel electrolyte.*

3.2.9 Characterisation of carrageenan-carbon composites using SEM

The sample studied using microscopy was prepared using the method described in ***Fig. 24 E***. Prior to the first microscopy experiment, the sample was dried in a vacuum over two days and subsequently stored for a few weeks in a laboratory, uncovered. The first experiment included the study of the composite's surface.

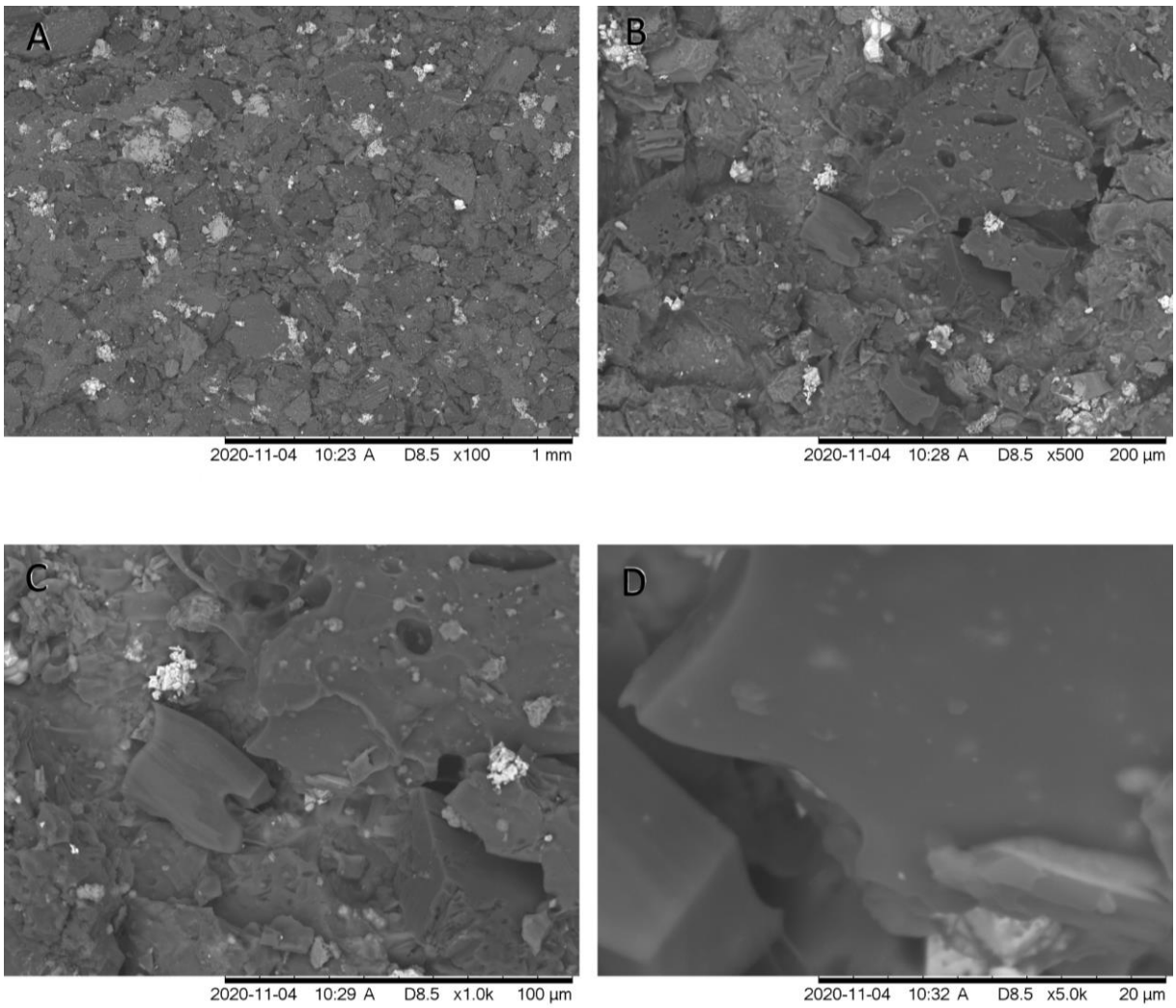

Figure 26. *The gained images of the composite sample's surface in* ***A.*** *100x* ***B.*** *500x* ***C.*** *1000x and* ***D.*** *2500x magnifications.*

After some time, the microscopy was performed on the film's cross-section. To obtain a clean cross-section, a piece of a composite film was frozen in liquid nitrogen and then cut using a scalpel. The composite was prepared anew and stored safely under cover, to check the suspicions of a contamination arising from the surface microscopy results. A sample of $CaCl_2$-carrageenan film with no carbon was also made and processed the same way, but due to residual water and apparently poor conductivity the gained image quality was too poor.

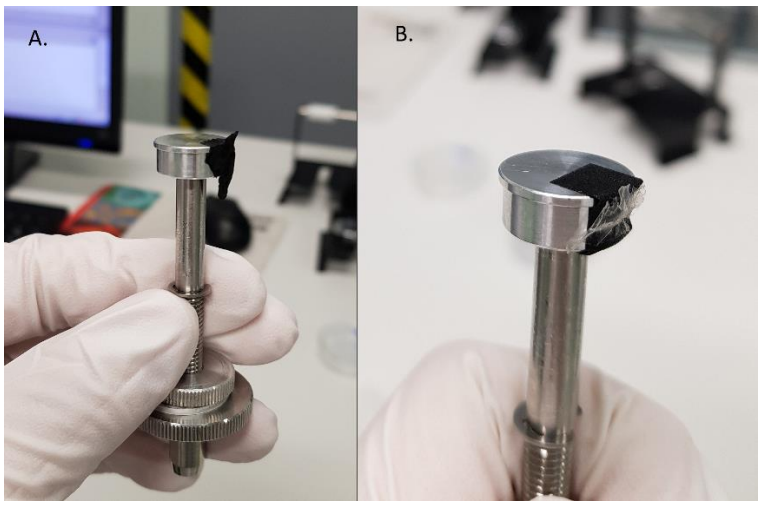

Figure 27. *The samples (**A**. dried carrageenan/carbon composite film and **B**. dried salt-cured carrageenan film) which cross-sections were studied during the experiment fixed on the holder using carbon tape. Pictures were taken right before the microscopy tests.*

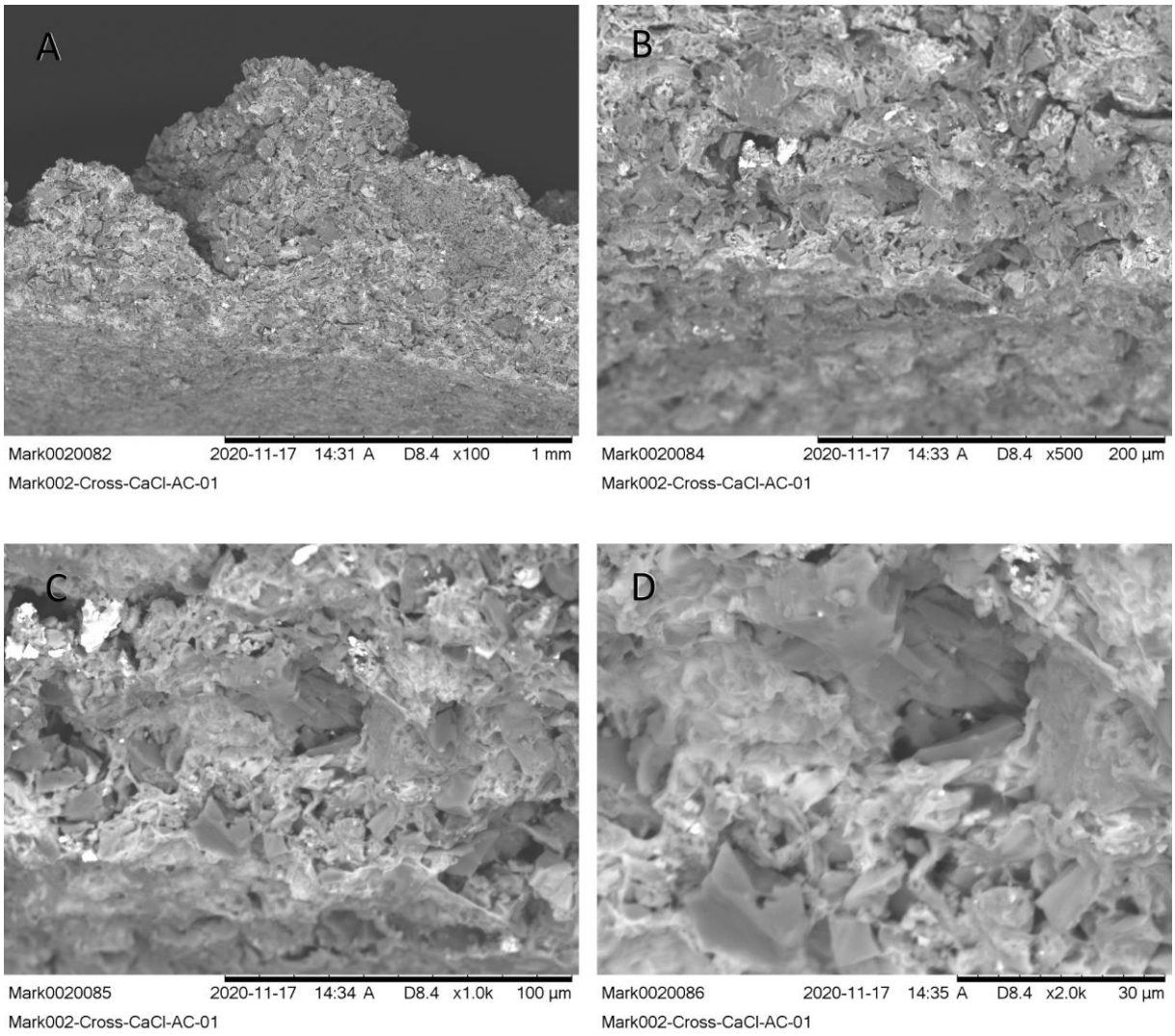

Figure 28. *The gained image of the cross-section of the composite under **A.** 100x, **B.** 500x, **C.** 1000x and **D.** 2000x magnifications. At magnifications higher than x2000 the image quality became insufficient with details being barely intelligible.*

The images gained from the microscopy show that the surface of created composites is uneven, with chunks (most likely, of the carbon) of various sizes being dispersed around it. The sizes of the chunks seemingly varied from about 150 or so um to approximately 10 μm in size.

The cross-section images showed the chunks of various sizes being dispersed through the resulting carrageenan film, once again showing the surface film to be quite uneven. The cross section also shows the presence of a quite high number of pores, which seems to be present in the carrageenan matrix.

The surface images also showed the presence of some less-conductive species dispersed on the top of the film, potentially some contamination, originating either from the lab environment or from the supplied materials.

3.2.10 Characterization of carrageenan components using EDX

In parallel with the microscopy analysis the same samples were also subjected to EDX spectroscopy. The first location of analysis selected was one of the big chunks seen in the surface images, which was focused upon closely and subjected to a scan with up to 15 kV accelerating voltage.

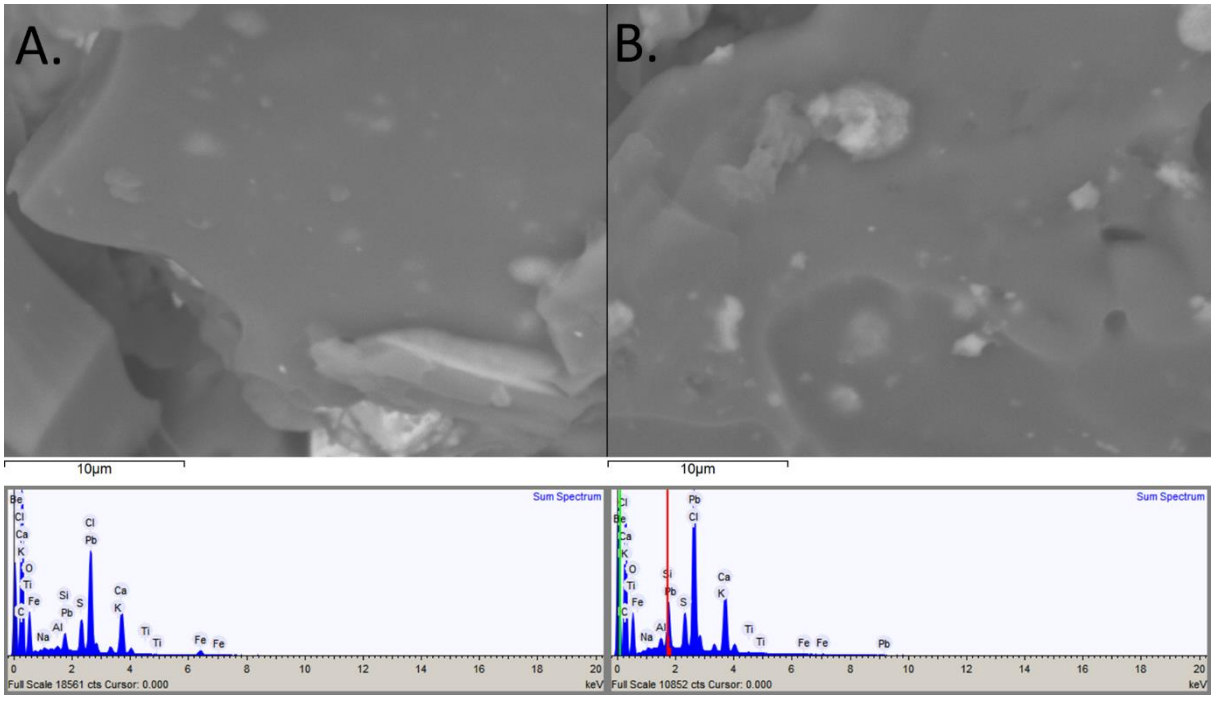

***Figure 29**. **A. On top:** the SEM image of the first chunk that was focused onto for the analysis. **On the bottom:** the sum spectrum of all the detected elements with corresponding energies. **B. On top: t**he SEM image of the second chunk analysed and the sum spectrum of all the detected elements and the corresponding energies for the peaks.*

Table 2. *The table of the summary results for the elemental analysis, both in the first and second scan location. Each element is given together with its total detected percentage of the weight as well as its total number percentage.*

	1st location		**2nd location**	
Element	Weight, %	Number of atoms, %	Weight, %	Number of atoms, %
Carbon	63.334	76.905	60.343	75.456
Oxygen	16.977	15.477	15.448	14.502
Sodium	0.146	0.092	0.131	0.086
Aluminum	0.148	0.080	0.386	0.215
Silicon	0.880	0.457	2.060	1.102
Sulfur	2.080	0.946	2.047	0.959
Chlorine	8.276	3.405	11.504	4.874
Potassium	0.664	0.248	0.652	0.251
Calcium	5.101	1.856	6.457	2.420
Titanium	0.108	0.033	0.124	0.039
Iron	1.786	0.466	0.193	0.052
Lead	0.499	0.035	0.655	0.047

The detected prevalence of carbon on the first chunk serves to support the previously made suggestion of the dispersed chunks being pieces of carbon of various sizes. Large presence of oxygen and sulfur is also to be expected, owing to the carbohydrate monomers of carrageenan and the organosulfate groups present in it. Calcium and chlorine being greatly present can be easily explained by the fact that calcium chloride solution was used to cure the film the part of which is present here, as well as by the deposition method which included covering of the carbon ink with the solution of the salt; moreover, the ratio of the total number of these elements is close to 1:2 ($\frac{Atomic\ \%\ (Ca)}{Atomic\ \%\ (Cl)} = \frac{1.856}{3.405} = 0.545$), as should be expected due to the chloride molecule composition. Small presence of iron and potassium was detected, most likely due to contamination of the sample because of long storage under open air. Additionally, traces of titanium and sodium were found, with a faint signal of lead, the latter likely due to an error as higher acceleration voltages would be required for proper detection of such a heavy element. Silica was also detected in a more or less significant amount, either present due to a contamination or coming from an impurity in one of the components used for the manufacturing, with activated carbon being the most likely candidate as it was not a lab-grade

reagent. Scans with mapped silica, carbon, oxygen, sulfur, calcium and chlorine were then performed to see their distribution.

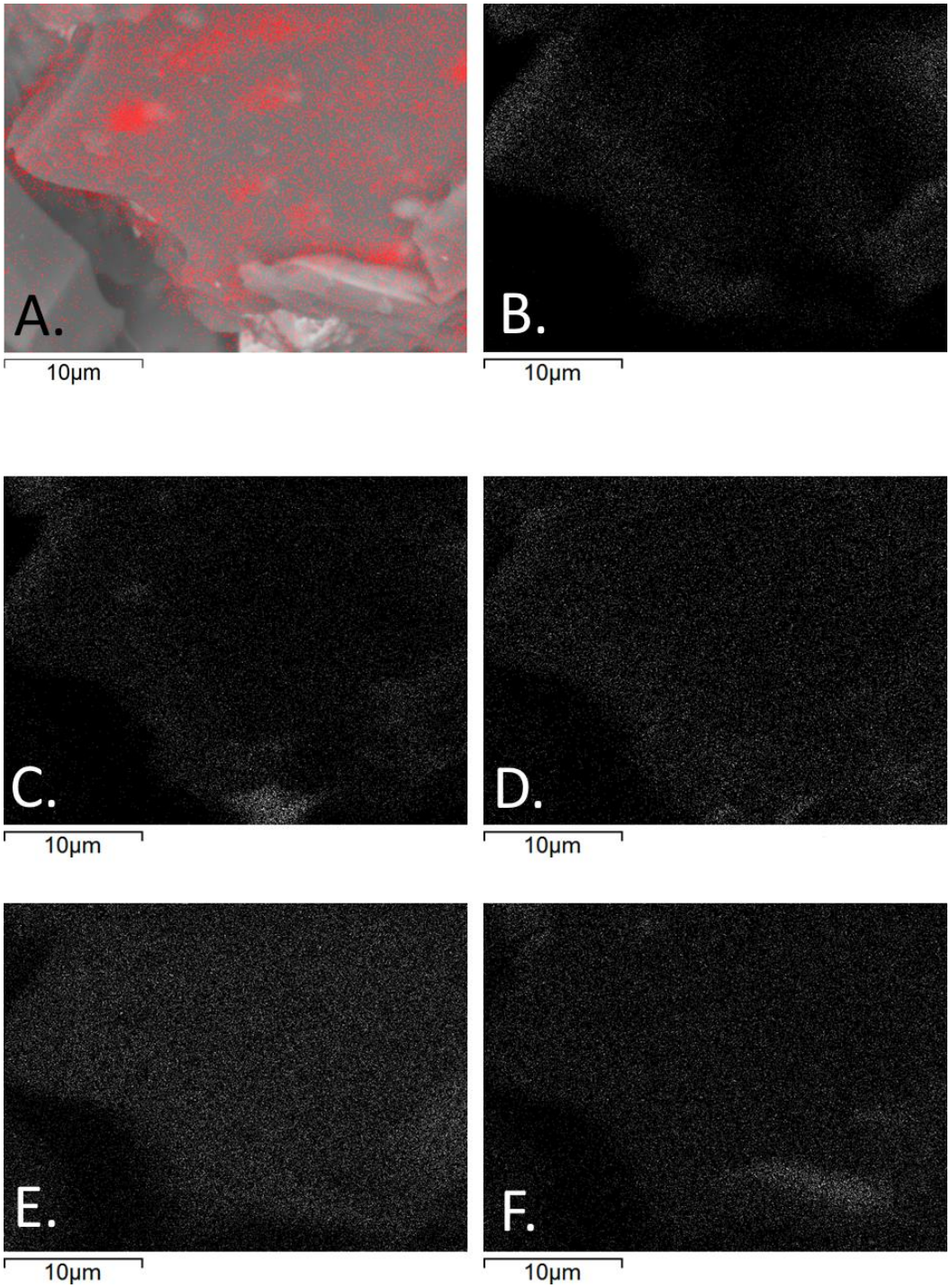

Figure 30. ***A.*** *A map of the detected silica (red) overlayed on the SEM image of the chunk.* ***B.*** *A map of the detected carbon.* ***C.*** *A map of the detected oxygen.* ***D.*** *A map of the detected sulfur.* ***E.*** *A map of the detected chlorine and* ***F.*** *a map of the detected calcium.*

As can be seen on the maps, sulfur and oxygen are somewhat dispersed over the chunk, but, just like carbon, seem to be covered by some other elements. Considering the seen dispersion of Ca and Cl in these maps, it seems possible that calcium chloride does indeed cover the part

of the surface of the film, laying on top of both the carbon and the carrageenan binder; especially since calcium seems to be greatly prominent in a small crystal-like object covering the carbon at the bottom of the picture (***Fig. 30 A, B and F***). Strange white spots of unknown origin seen on the SEM image seem to correspond to the spots with large silica concentration, some of them also having a large presence of oxygen. Still, some doubts about the precision of these conclusions remained, with a possibility of brightness due to greater proximity influencing the signal of the crystal-like chunk attributed to some chloride residue. So, another location on the film (***Fig. 29 B***) was chosen and subjected to the same analysis (***Fig. 31***).

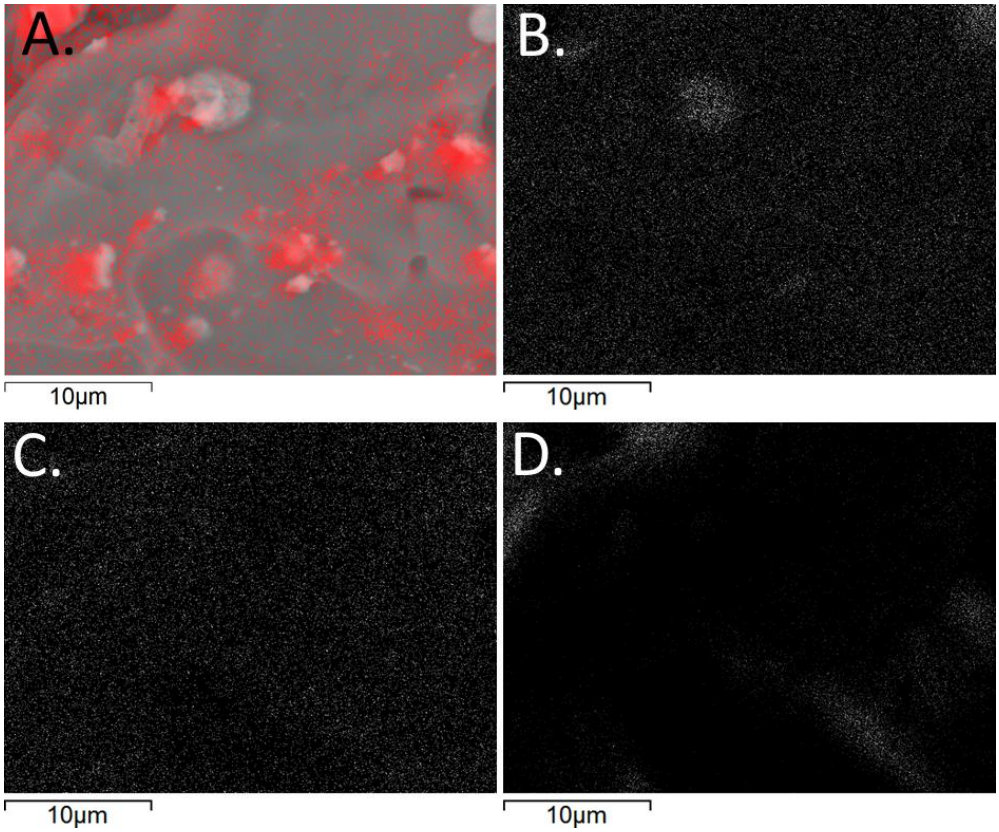

Figure 31. A. *The map of detected silica (red) overlayed on the SEM image of the scan location.* ***B.*** *The map of detected calcium.* ***C.*** *The map of detected sulfur.* ***D.*** *The map of detected carbon.*

As suggested before, the strange white spots on the carbon chunks seem to consist of silicon, with some carbon residues also present as small crystalline pieces. Carbon seems to be once again covered with some other element, potentially, carrageenan binder and the salt.

The same analysis was later performed on the cross-sections of the film (***Fig. 32, Fig. 33***).

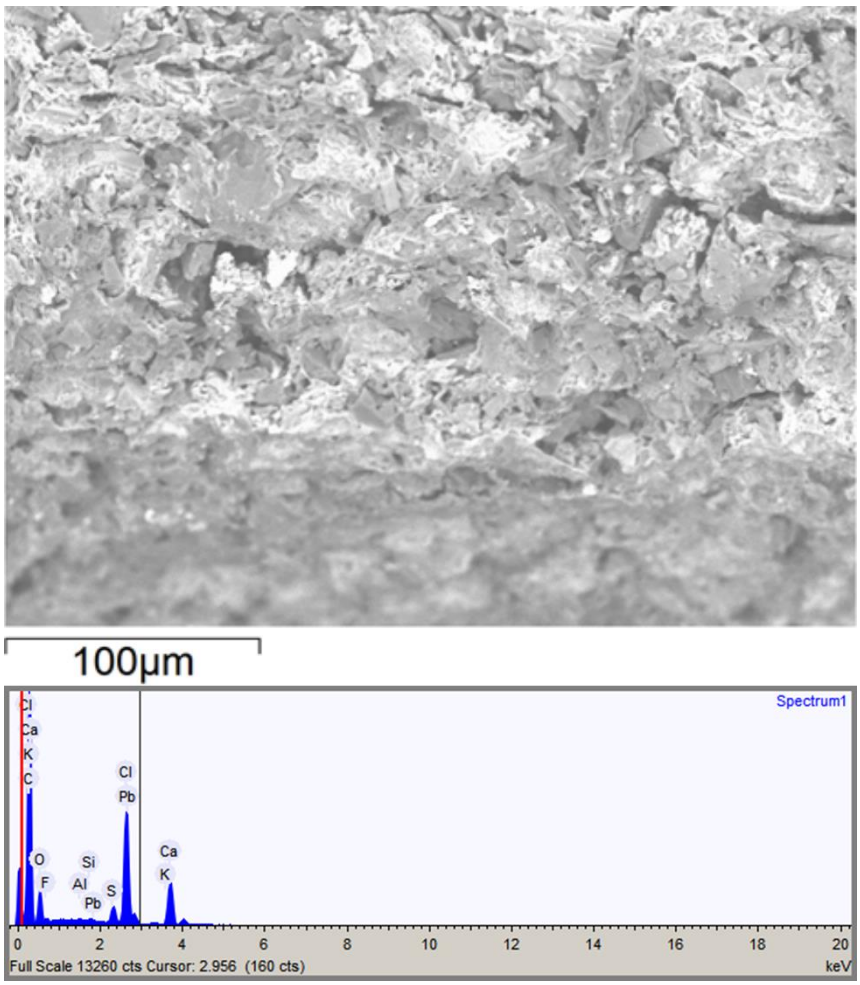

***Figure 32**. The SEM image of the film's cross-section and the summary spectrum of the detected elements with corresponding energies of the peaks.*

***Table 3.** The table of the summary results for the elemental analysis of the film's cross-section. The data is presented in a form the percentage of the total weight and the total number of atoms in percentage.*

Element	**Weight, %**	**Number of atoms, %**
Carbon	70.947	82.072
Oxygen	13.394	11.633
Fluorine	1.250	0.914
Aluminum	0.061	0.031
Silicon	0.117	0.058
Sulfur	0.921	0.399
Chlorine	8.264	3.239
Potassium	0.098	0.035
Calcium	4.603	1.596
Lead	0.344	0.023

The prevalence of carbon seems to once again support the idea of the dispersed chunks originating from the activated carbon. Potassium, silica, aluminum seem to be present in traces, potentially indicating that higher presence of Si and K on the surface did come from contamination due to improper storage. The presence of sulfur on oxygen was smaller, suggesting that the carrageenan binder was more present on the surface of the film. Calcium and chlorine had a significant presence, too, once again being in a numerical ratio of near 1:2 ($\frac{1.596}{3.239} = 0.493$), supporting the idea of their salt origins and showing good diffusion of the salt into the composite film. Of interest is an inexplicable presence of fluorine in the sample (~1% of total atomic number), possibly, due to some contamination or error in the analysis.

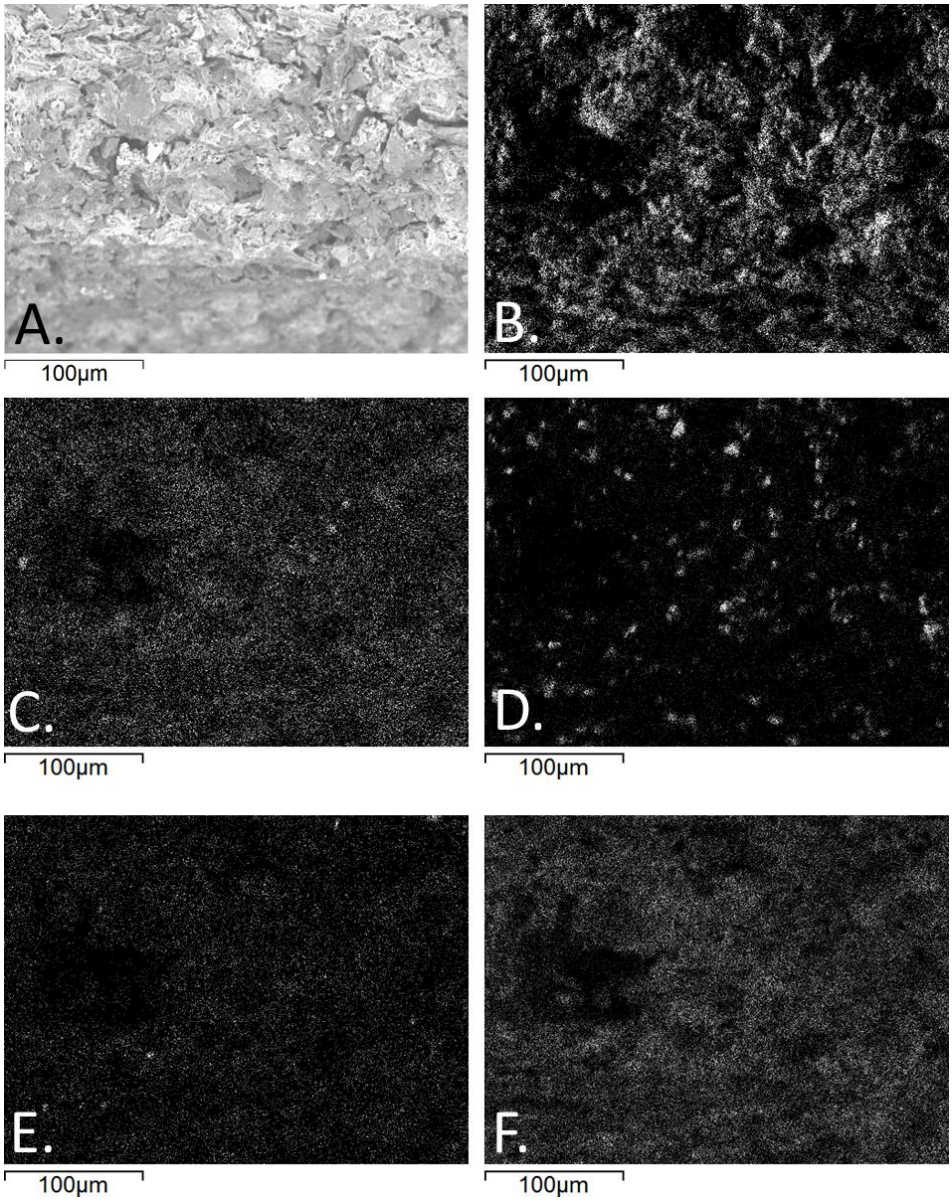

Figure 33. ***A.*** *The SEM image of the cross-section used in the spectroscopy.* ***B.*** *The map of the detected carbon.* ***C.*** *The map of the detected calcium.* ***D.*** *The map of the detected silicon.* ***E.*** *The map of the detected sulfur.* ***F.*** *The map of the detected chlorine.*

3.2.11 Modification of carbon electrodes with carrageenan

To determine whether the produced activated carbon-carrageenan composites are conductive, CV and EIS were performed. Utilizing the prototype of the designed printed cell, an electrochemical cell was set up with the sample being a cut piece of the dried film previously characterized using microscopy. A 5 mM ferro-/ferricyanide solution in 7.4 pH PB was used as the electrolyte and Pt grid and Ag/AgCl/(3M KCl) served as the counter and reference, respectively. Unfortunately, the gained results showed poor conductivity of the sample, and after it was extracted from the cell to perform some manipulations on the latter in-between the runs, it was found to be greatly swollen to the point that the reassembly of the cell was impossible (***Fig***. ***34***).

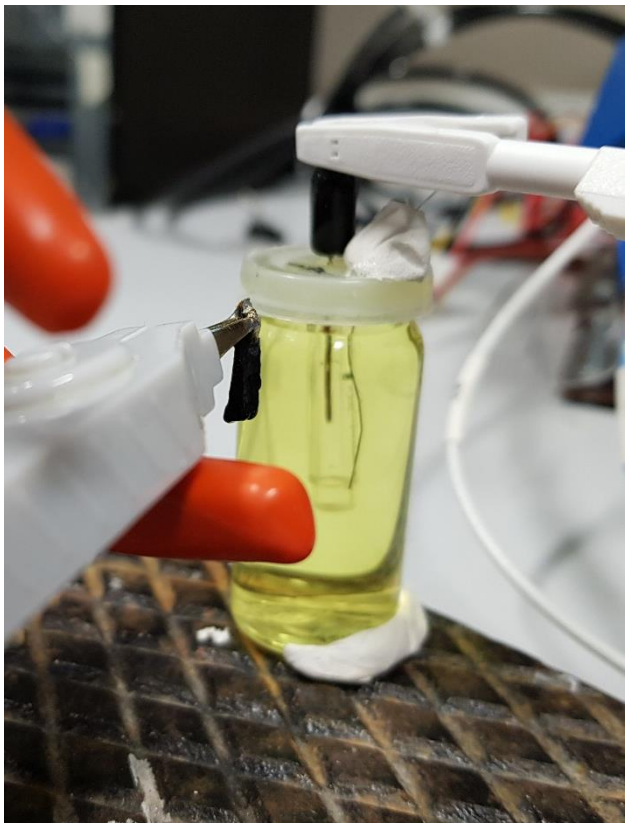

Figure 34. *The swollen sample and the setup used in the analysis in the background.*

After some considerations and discussions, insufficient area of the electric connection to the composite was suggested to be the most likely reason for poor performance, as conductive polymers generally require high contact areas. Additionally, there was a need to account for the wetting and sampling of the composite, so a new setup was designed.

Two electrodes were assembled out of carbon fibre bundles and their dimensions were measured (***Table 4***), although during the manipulations that followed, many fibres fell out of the bundles, possibly invalidating this data.

Table 4. *The dimension values for the manufactured electrodes*

	Active area length, mm	Bundle thickness averaged over 10 measurements, mm
WE	53	0.0469
CE	58	0.0517

The carrageenan-carbon ink was prepared as follows (***Fig. 24 F***): 1.5% water and κ-car mixture were mixed with crushed activated carbon in a 10:1 ratio. The resulting slurry was mixed for a day using a magnetic stirrer on 60 Celsius. The vial for the ink was purposefully chosen to be not much wider than the stirring bead to ensure proper mechanical influence on the carbon powder particles.

An electrochemical cell was assembled using the 3D printed electrochemical cap and CV and EIS were done first in a 7-pH potassium phosphate buffer and then in a 5 mM solution of ferrocyanide and ferricyanide pair in the same buffer. An Ag/AgCl/(3 M KCl) electrode was used as a reference.

After the measurements were performed in a ferro/ferricyanide solution on a clean fibre-bundle WE, the latter was extracted, washed with mQ water, and coated with a mix of k-carrageenan and activated carbon, with the resulting membrane cover additionally smeared with 0.9M CaCl2 solution to make it cure. The WE was then allowed to dry for a few minutes and reinserted into the cell, after which CV and EIS were performed again.

All the voltammetry scans were done between the -1 and +1 V potentials on the 20 mV/s scan rate. The EIS was done on a 10 mV potential on the frequencies varied from 100 kHz to 0.1 Hz.

As can be seen from the gained CVs (***Fig. 35***) alone, the ion-cured composite membranes do show fine ion permeability. The half-wave potential has increased (***Table 5***) and the distance between the peaks grew smaller for the sample with the membrane; however, the fibres were

not washed with water which has likely affected the peak separation for the clean fibres in the ferro/ferry electrolyte.

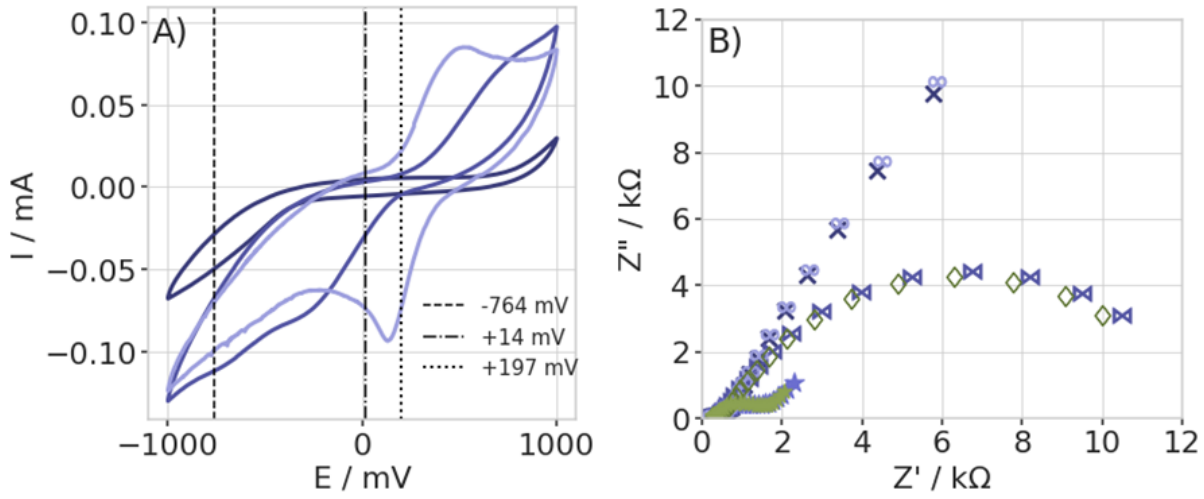

***Figure 35. A**. The gained voltammograms. Dark blue is the phosphate buffer measurement, blue and lilac are ferro/ferricyanide scans for the clean and membrane-covered buffers, respectively. The lines on the graph correspond to the potentials of redox reactions detected during the previous CFMB in PB scans performed. 197 mV corresponds to the OCP potential. **B**. The EIS curves and the close-up of the high-frequency zone (bottom). The blue crosses are the scan in the phosphate buffer, green diamonds and stars are the curves for the clean and membrane-covered fibres in ferrocene, respectively.*

***Table 5.** Half-wave potentials and peak-to-peak separations for the measured CVs.*

	CF in ferrocene	Membrane-covered CF in ferrocene
$E_{1/2}$, V	0.22245	0.31465
E_p, V	0.9529	0.3517

The EIS results (***Fig. 35 B***) showed a lack of a well-distinguishable semicircle in the high-frequency regions for scans in blank PB buffer and clean CF in ferrocene, possibly indicating either some measurement error or that the charge transfers in the cell were prevalently limited by diffusion. For the phosphate buffer measurement, the lack of electroactive species might have led to a very high diffusion-controlled impedance in low-frequency regions. The

measurement for the membrane-covered fibres showed that the coating decreased the total impedance, with a discernible semicircle spanning mid to low-mid frequencies, possibly coming from reaction resistance on the composite's surface. Highest frequencies still had no clear semicircle, but a short somewhat horizontal line. It seems that the membrane does allow for good transfer of charges and reaches a diffusion-controlled impedance at lower frequencies. It is worth noting that the gained EIS results correspond to earlier results for the same CFMB in PB in magnitude (***Fig. 12 A***)

3.2.12 Conclusions

- Non-modified commercial carbon fiber microcylinder bundles were successfully electrochemically characterized as an electrode.
- The fabricated electrodes were used without any additional surface treatment, activation or modification; the gained results indicate good cycling stability and diffusion coefficient ($6.66 \pm 1.02 \times 10^{-6}$ cm^2/s) and relaxation time constant ($\tau^{-1} = 71$ s^{-1}) comparable to data for screen-printed carbon electrodes.
- The linear range of the sensitivity of the CFMB sensor to dopamine was found to be 0 to 100 μM, with the LOD calculated to have an adequate value of 8.85 LOD. This allows for such a simple, low-cost and disposable electrode to be used for detection of some other analytes (e.g., ascorbic acid, glucose) or as a matrix for soft robots. Namely, the latter use would introduce a new and prospective technique for electrochemical sensing-based actuator designs able to be incorporated into the neural signalling system of a living being.
- K-carrageenan was found to be a convenient biodegradable matrix for composites; carbon-carrageenan composites, in particular.
- Ease of shaping and dispersing of the additives serves to make the production of such materials very simple, with possibilities of manufacture of both coatings and self-standing films with ordinary, conventional tools. Good dispersion of carbon is supported by the gained images of the composite film cross-sections using SEM, with images of the surface indicating strong variation of the dispersed carbon chunk size.
- The proposed rapidly and controllably reversible gelation of κ-car was not achieved during the work: it can be suggested that the strength binding of the carrageenan aggregation organosulfate and cations (both Ca^{2+} and K^{+}) cannot be overcome by current alone, and would require some additional influence, such as enzymatic or similar biological activity, changes in pH or melting of the gel.
- The composite coatings manufactured during the work showed good ionic permeability, relatively low reaction resistance on high to low-mid voltage frequencies and seemingly

diffusion-controlled impedance over mid-low to low voltage frequencies for the frequencies between 100 kHz to 0.1 Hz, at least in a state of maximum swelling.

- Of note is a seemingly outstanding ability of the produced films to swell after a thorough drying, with noticeable changes in size, though the attempts made to measure the exact intake of liquid failed due to intensive crumbling of the sample that started to happen.

SUMMARY

During this work, the following results were accomplished:

1. An electrochemical cell usable in conjunction with flexible high-area electrodes was designed and produced using 3D printing. Unfortunately, the utilized NinjaFlex filament, consisting mostly of polyurethane resins, was poorly biodegradeable.
2. The used flexible high-area electrodes were successfully characterized using microscopy and electrochemistry.
3. The flexible high-area electrodes were successfully characterized for biosensing of dopamine in 7.4 pH PB.
4. The suggested current-controlled rapid reversibility of metal-cation induced gelation in carrageenans was not achieved during this work. It is suggested that the current alone is insufficient to reverse the gelation.
5. Composite coatings and self-standing films were successfully made from consumer-grade activated carbon and κ-carrageenan. The method of production was optimized and is presented in the results and discussion part of the work.
6. The manufactured composites were characterised using SEM, EDX and electrochemistry. The electrochemical experiments indicate diffusion-limited conductivity and good ionic permeability, while SEM and EDX suggest good dispersion of carbon in the carrageenan matrix and presence of carbon chunks of various sizes.
7. A soft actuator was designed based on an already existing EDLC-like design incorporating the assumed property of carrageenans to gelate reversibly under current. As the such a property was achieved during this work, the practical implementation of such a design remained unexecuted.

REFERENCES

(1) Pacheco-Quito, E.-M.; Ruiz-Caro, R.; Veiga, M.-D. Carrageenan: Drug Delivery Systems and Other Biomedical Applications. *Mar. Drugs* **2020**, *18* (11), 583. https://doi.org/10.3390/md18110583.

(2) Campo, V. L.; Kawano, D. F.; Silva, D. B. da; Carvalho, I. Carrageenans: Biological Properties, Chemical Modifications and Structural Analysis - A Review. *Carbohydrate Polymers*. 2009. https://doi.org/10.1016/j.carbpol.2009.01.020.

(3) Bui, V. T. N. T.; Nguyen, B. T.; Renou, F.; Nicolai, T. Structure and Rheological Properties of Carrageenans Extracted from Different Red Algae Species Cultivated in Cam Ranh Bay, Vietnam. *J. Appl. Phycol.* **2019**. https://doi.org/10.1007/s10811-018-1665-1.

(4) Pinheiro, A. C.; Bourbon, A. I.; Quintas, M. A. C.; Coimbra, M. A.; Vicente, A. A. K-Carrageenan/Chitosan Nanolayered Coating for Controlled Release of a Model Bioactive Compound. *Innov. Food Sci. Emerg. Technol.* **2012**, *16*, 227–232. https://doi.org/10.1016/j.ifset.2012.06.004.

(5) Martins, A. F.; Vlcek, J.; Wigmosta, T.; Hedayati, M.; Reynolds, M. M.; Popat, K. C.; Kipper, M. J. Chitosan/Iota-Carrageenan and Chitosan/Pectin Polyelectrolyte Multilayer Scaffolds with Antiadhesive and Bactericidal Properties. *Appl. Surf. Sci.* **2020**. https://doi.org/10.1016/j.apsusc.2019.144282.

(6) Zhang, C.; Sun, G.; Cao, L.; Wang, L. Accurately Intelligent Film Made from Sodium Carboxymethyl Starch/κ-Carrageenan Reinforced by Mulberry Anthocyanins as an Indicator. *Food Hydrocoll.* **2020**. https://doi.org/10.1016/j.foodhyd.2020.106012.

(7) Pérez-Madrigal, M. M.; Estrany, F.; Armelin, E.; Díaz, D. D.; Alemán, C. Towards Sustainable Solid-State Supercapacitors: Electroactive Conducting Polymers Combined with Biohydrogels. *J. Mater. Chem. A* **2016**. https://doi.org/10.1039/c5ta08680a.

(8) Li, D.; Yang, D.; Yang, X.; Wang, Y.; Guo, Z.; Xia, Y.; Sun, S.; Guo, S. Double-Helix Structure in Carrageenan-Metal Hydrogels: A General Approach to Porous Metal Sulfides/Carbon Aerogels with Excellent Sodium-Ion Storage. *Angew. Chemie Int. Ed.* **2016**, *55* (51), 15925–15928. https://doi.org/10.1002/anie.201610301.

(9) Farhana, N. K.; Omar, F. S.; Shanti, R.; Mahipal, Y. K.; Ramesh, S.; Ramesh, K. Iota-Carrageenan-Based Polymer Electrolyte: Impact on Ionic Conductivity with Incorporation of AmNTFSI Ionic Liquid for Supercapacitor. *Ionics (Kiel).* **2019**.

https://doi.org/10.1007/s11581-019-02865-1.

(10) Rudhziah, S.; Rani, M. S. A.; Ahmad, A.; Mohamed, N. S.; Kaddami, H. Potential of Blend of Kappa-Carrageenan and Cellulose Derivatives for Green Polymer Electrolyte Application. *Ind. Crops Prod.* **2015**. https://doi.org/10.1016/j.indcrop.2014.12.051.

(11) Quignard, F.; Valentin, R.; Di Renzo, F. Aerogel Materials from Marine Polysaccharides. *New Journal of Chemistry*. 2008. https://doi.org/10.1039/b808218a.

(12) Patil, R. T.; Speaker, T. J. Carrageenan as an Anionic Polymer for Aqueous Microencapsulation. *Drug Deliv.* **1998**, *5* (3), 179–182. https://doi.org/10.3109/10717549809052033.

(13) Liu, S.; Li, L. Thermoreversible Gelation and Scaling Behavior of Ca 2+ -Induced κ-Carrageenan Hydrogels. *Food Hydrocoll.* **2016**, *61*, 793–800. https://doi.org/10.1016/j.foodhyd.2016.07.003.

(14) ZABIK, M. E.; ALDRICH, P. J. Gel Strength of Kappa-Carrageenan as Affected by Cations. *J. Food Sci.* **1968**, *33* (4), 371–377. https://doi.org/10.1111/j.1365-2621.1968.tb03632.x.

(15) Running, C. A.; Falshaw, R.; Janaswamy, S. Trivalent Iron Induced Gelation in Lambda-Carrageenan. *Carbohydr. Polym.* **2012**. https://doi.org/10.1016/j.carbpol.2011.11.018.

(16) Hermansson, A.-M.; Eriksson, E.; Jordansson, E. Effects of Potassium, Sodium and Calcium on the Microstructure and Rheological Behaviour of Kappa-Carrageenan Gels. *Carbohydr. Polym.* **1991**, *16* (3), 297–320. https://doi.org/10.1016/0144-8617(91)90115-S.

(17) Liu, S.; Huang, S.; Li, L. Thermoreversible Gelation and Viscoelasticity of κ-Carrageenan Hydrogels. *J. Rheol. (N. Y. N. Y).* **2016**. https://doi.org/10.1122/1.4938525.

(18) Perez, S. J. L. P.; Claudio, G. C. Molecular Dynamics Simulations of Two Double-Helical Hexamer Fragments of Iota-Carrageenan in Aqueous Solution. *J. Mol. Graph. Model.* **2020**. https://doi.org/10.1016/j.jmgm.2020.107588.

(19) Morris, E. R.; Rees, D. A.; Robinson, G. Cation-Specific Aggregation of Carrageenan Helices: Domain Model of Polymer Gel Structure. *J. Mol. Biol.* **1980**, *138* (2), 349–362. https://doi.org/10.1016/0022-2836(80)90291-0.

(20) Glavatskih, S.; Höglund, E. Tribotronics—Towards Active Tribology. *Tribol. Int.* **2008**, *41* (9–10), 934–939. https://doi.org/10.1016/j.triboint.2007.03.001.

(21) Boyraz, P.; Runge, G.; Raatz, A. An Overview of Novel Actuators for Soft Robotics.

High-Throughput **2018**, *7* (3), 1–21. https://doi.org/10.3390/act7030048.

(22) Kaasik, F.; Must, I.; Baranova, I.; Põldsalu, I.; Lust, E.; Johanson, U.; Punning, A.; Aabloo, A. Scalable Fabrication of Ionic and Capacitive Laminate Actuators for Soft Robotics. *Sensors Actuators, B Chem.* **2017**, *246*, 154–163. https://doi.org/10.1016/j.snb.2017.02.065.

(23) Cėpla, V.; Rakickas, T.; Stankevičienė, G.; Mazėtytė-Godienė, A.; Baradokė, A.; Ruželė, Ž.; Valiokas, R. Photografting and Patterning of Poly(Ethylene Glycol) Methacrylate Hydrogel on Glass for Biochip Applications. *ACS Appl. Mater. Interfaces* **2020**, *12* (29), 32233–32246. https://doi.org/10.1021/acsami.0c04085.

(24) Sudhof, T. C. Calcium Control of Neurotransmitter Release. *Cold Spring Harb. Perspect. Biol.* **2012**, *4* (1), a011353–a011353. https://doi.org/10.1101/cshperspect.a011353.

(25) KATZ, B.; MILEDI, R. Ionic Requirements of Synaptic Transmitter Release. *Nature* **1967**, *215* (5101), 651–651. https://doi.org/10.1038/215651a0.

(26) Neher, E.; Sakaba, T. Multiple Roles of Calcium Ions in the Regulation of Neurotransmitter Release. *Neuron* **2008**, *59* (6), 861–872. https://doi.org/10.1016/j.neuron.2008.08.019.

(27) Sibille, J.; Dao Duc, K.; Holcman, D.; Rouach, N. The Neuroglial Potassium Cycle during Neurotransmission: Role of Kir4.1 Channels. *PLOS Comput. Biol.* **2015**, *11* (3), e1004137. https://doi.org/10.1371/journal.pcbi.1004137.

(28) Geiger, J. R. P.; Jonas, P. Dynamic Control of Presynaptic Ca2+ Inflow by Fast-Inactivating K+ Channels in Hippocampal Mossy Fiber Boutons. *Neuron* **2000**, *28* (3), 927–939. https://doi.org/10.1016/S0896-6273(00)00164-1.

(29) Han, J.; Cui, Y.; Han, X.; Liang, C.; Liu, W.; Luo, D.; Yang, D. Super-Soft DNA/Dopamine-Grafted-Dextran Hydrogel as Dynamic Wire for Electric Circuits Switched by a Microbial Metabolism Process. *Adv. Sci.* **2020**, *7* (13), 2000684. https://doi.org/10.1002/advs.202000684.

(30) Cao, J.; Zhou, Z.; Song, Q.; Chen, K.; Su, G.; Zhou, T.; Zheng, Z.; Lu, C.; Zhang, X. Ultrarobust Ti 3 C 2 T x MXene-Based Soft Actuators via Bamboo-Inspired Mesoscale Assembly of Hybrid Nanostructures. *ACS Nano* **2020**, *14* (6), 7055–7065. https://doi.org/10.1021/acsnano.0c01779.

(31) Booklet | Brain-Inspired Intelligent Robotics: The Intersection of Robotics and

Neuroscience Sciences. *Science (80-.).* **2016**, *354* (6318), 1445.2-1445. https://doi.org/10.1126/science.354.6318.1445-b.

(32) Cao, J.; Liang, W.; Zhu, J.; Ren, Q. Control of a Muscle-like Soft Actuator via a Bioinspired Approach. *Bioinspir. Biomim.* **2018**, *13* (6), 066005. https://doi.org/10.1088/1748-3190/aae1be.

(33) Park, H.; Lee, Y.; Kim, N.; Seo, D.; Go, G.; Lee, T. Flexible Neuromorphic Electronics for Computing, Soft Robotics, and Neuroprosthetics. *Adv. Mater.* **2020**, *32* (15), 1903558. https://doi.org/10.1002/adma.201903558.

(34) Bing, Z.; Meschede, C.; Röhrbein, F.; Huang, K.; Knoll, A. C. A Survey of Robotics Control Based on Learning-Inspired Spiking Neural Networks. *Front. Neurorobot.* **2018**, *12*. https://doi.org/10.3389/fnbot.2018.00035.

(35) Evans, R. Reinforcement Learning in a Neurally Controlled Robot Using Dopamine Modulated STDP, Imperial College London, 2015.

(36) Samson, R. D.; Frank, M. J.; Fellous, J.-M. Computational Models of Reinforcement Learning: The Role of Dopamine as a Reward Signal. *Cogn. Neurodyn.* **2010**, *4* (2), 91–105. https://doi.org/10.1007/s11571-010-9109-x.

(37) Budai, D. Carbon Fiber-Based Microelectrodes and Microbiosensors. In *Intelligent and Biosensors*; 2010. https://doi.org/10.5772/7158.

(38) Armstrong-James, M.; Millar, J. Carbon Fibre Microelectrodes. *J. Neurosci. Methods* **1979**. https://doi.org/10.1016/0165-0270(79)90039-6.

(39) Ponchon, J. L.; Cespuglio, R.; Gonon, F.; Jouvet, M.; Pujol1, J. F. Normal Pulse Polarography with Carbon Fiber Electrodes for in Vitro and in Vivo Determination of Catecholamines. *Anal. Chem.* **1979**. https://doi.org/10.1021/ac50045a030.

(40) Huffman, M. L.; Venton, B. J. Carbon-Fiber Microelectrodes for in Vivo Applications. *Analyst*. 2009. https://doi.org/10.1039/b807563h.

(41) Chatard, C.; Sabac, A.; Moreno-Velasquez, L.; Meiller, A.; Marinesco, S. Minimally Invasive Microelectrode Biosensors Based on Platinized Carbon Fibers for in Vivo Brain Monitoring. *ACS Cent. Sci.* **2018**. https://doi.org/10.1021/acscentsci.8b00797.

(42) Gonon, F.; Buda, M.; Cespuglio, R.; Jouvet, M.; Pujol, J. F. In Vivo Electrochemical Detection of Catechols in the Neostriatum of Anaesthetized Rats: Dopamine or DOPAC? *Nature* **1980**. https://doi.org/10.1038/286902a0.

(43) Cheng, Q.; Tang, J.; Ma, J.; Zhang, H.; Shinya, N.; Qin, L. C. Polyaniline-Coated

Electro-Etched Carbon Fiber Cloth Electrodes for Supercapacitors. *J. Phys. Chem. C* **2011**. https://doi.org/10.1021/jp203852p.

(44) Gomadam, P. M.; Weidner, J. W. Analysis of Electrochemical Impedance Spectroscopy in Proton Exchange Membrane Fuel Cells. *International Journal of Energy Research*. 2005. https://doi.org/10.1002/er.1144.

(45) Budai, D.; Molnár, Z. Novel Carbon Fiber Microeletrodes for Extracellular Electrophysiology. *Acta Biol. Szeged.* **2001**, *45* (1–4), 65–73.

(46) Cheer, J. F.; Aragona, B. J.; Heien, M. L. A. V.; Seipel, A. T.; Carelli, R. M.; Wightman, R. M. Coordinated Accumbal Dopamine Release and Neural Activity Drive Goal-Directed Behavior. *Neuron* **2007**. https://doi.org/10.1016/j.neuron.2007.03.021.

(47) Sanford, A. L.; Morton, S. W.; Whitehouse, K. L.; Oara, H. M.; Lugo-Morales, L. Z.; Roberts, J. G.; Sombers, L. A. Voltammetric Detection of Hydrogen Peroxide at Carbon Fiber Microelectrodes. *Anal. Chem.* **2010**. https://doi.org/10.1021/ac100536s.

(48) Malinski, T.; Taha, Z. Nitric Oxide Release from a Single Cell Measured in Situ by a Porphyrinic-Based Microsensor. *Nature* **1992**. https://doi.org/10.1038/358676a0.

(49) Rice, M. E. H2O2: A Dynamic Neuromodulator. *Neuroscientist*. 2011. https://doi.org/10.1177/1073858411404531.

(50) Jimenez Del Rio, M.; Velez-Pardo, C. The Hydrogen Peroxide and Its Importance in Alzheimer's and Parkinson's Disease. *Current Medicinal Chemistry - Central Nervous System Agents*. 2004. https://doi.org/10.2174/1568015043356896.

(51) Brisch, R.; Saniotis, A.; Wolf, R.; Bielau, H.; Bernstein, H. G.; Steiner, J.; Bogerts, B.; Braun, K.; Kumaratilake, J.; Henneberg, M.; Gos, T. The Role of Dopamine in Schizophrenia from a Neurobiological and Evolutionary Perspective: Old Fashioned, but Still in Vogue. *Frontiers in Psychiatry*. 2014. https://doi.org/10.3389/fpsyt.2014.00047.

(52) Leonard, B. E. Chapter 9 Biological Aspects of Depression; 2000; pp 179–205. https://doi.org/10.1016/S1569-2582(00)80011-2.

(53) Nutt, D.; Demyttenaere, K.; Janka, Z.; Aarre, T.; Bourin, M.; Canonico, P. L.; Carrasco, J. L.; Stahl, S. The Other Face of Depression, Reduced Positive Affect: The Role of Catecholamines in Causation and Cure. *Journal of Psychopharmacology*. 2007. https://doi.org/10.1177/0269881106069938.

(54) Palmer, R. M. J.; Ferrige, A. G.; Moncada, S. Nitric Oxide Release Accounts for the Biological Activity of Endothelium-Derived Relaxing Factor. *Nature* **1987**.

https://doi.org/10.1038/327524a0.

(55) Furchgott, R. F.; Zawadzki, J. V. The Obligatory Role of Endothelial Cells in the Relaxation of Arterial Smooth Muscle by Acetylcholine. *Nature* **1980**. https://doi.org/10.1038/288373a0.

(56) Vanhoutte, P. M. Endothelial Dysfunction and Atherosclerosis. *Eur. Heart J.* **1997**. https://doi.org/10.1016/S0195-668X(97)90005-1.

(57) Wei, E. P.; Kontos, H. A.; Christman, C. W.; DeWitt, D. S.; Povlishock, J. T. Superoxide Generation and Reversal of Acetylcholine-Induced Cerebral Arteriolar Dilation after Acute Hypertension. *Circ. Res.* **1985**. https://doi.org/10.1161/01.RES.57.5.781.

(58) Pieper, G. M.; Gross, G. J. Oxygen Free Radicals Abolish Endothelium-Dependent Relaxation in Diabetic Rat Aorta. *Am. J. Physiol. - Hear. Circ. Physiol.* **1988**. https://doi.org/10.1152/ajpheart.1988.255.4.h825.

(59) De Vriese, A. S.; Verbeuren, T. J.; Van De Voorde, J.; Lameire, N. H.; Vanhoutte, P. M. Endothelial Dysfunction in Diabetes. *British Journal of Pharmacology*. 2000. https://doi.org/10.1038/sj.bjp.0703393.

(60) Cavalcanti, I. T.; Silva, B. V. M.; Peres, N. G.; Moura, P.; Sotomayor, M. D. P. T.; Guedes, M. I. F.; Dutra, R. F. A Disposable Chitosan-Modified Carbon Fiber Electrode for Dengue Virus Envelope Protein Detection. *Talanta* **2012**. https://doi.org/10.1016/j.talanta.2012.01.002.

(61) Heien, M. L. A. V.; Phillips, P. E. M.; Stuber, G. D.; Seipel, A. T.; Wightman, R. M. Overoxidation of Carbon-Fiber Microelectrodes Enhances Dopamine Adsorption and Increases Sensitivity. *Analyst* **2003**. https://doi.org/10.1039/b307024g.

(62) Sekar, M.; Pandiaraj, M.; Bhansali, S.; Ponpandian, N.; Viswanathan, C. Carbon Fiber Based Electrochemical Sensor for Sweat Cortisol Measurement. *Sci. Rep.* **2019**, *9* (1), 403. https://doi.org/10.1038/s41598-018-37243-w.

(63) Anastasova, S.; Crewther, B.; Bembnowicz, P.; Curto, V.; Ip, H. M.; Rosa, B.; Yang, G.-Z. A Wearable Multisensing Patch for Continuous Sweat Monitoring. *Biosens. Bioelectron.* **2017**, *93*, 139–145. https://doi.org/10.1016/j.bios.2016.09.038.

(64) Kamei, T.; Tsuda, T.; Kitagawa, S.; Naitoh, K.; Koji Nakashima; Ohhashi, T. Physical Stimuli and Emotional Stress-Induced Sweat Secretions in the Human Palm and Forehead. *Anal. Chim. Acta* **1998**, *365* (1–3), 319–326. https://doi.org/10.1016/S0003-2670(97)00642-9.

(65) Mendes, D. G.; Iusim, M.; Angel, D.; Rotem, A.; Mordehovich, D.; Roffman, M.; Lieberson, S.; Boss, J. Ligament and Tendon Substitution with Composite Carbon Fiber Strands. *J. Biomed. Mater. Res.* **1986**, *20* (6), 699–708. https://doi.org/10.1002/jbm.820200604.

(66) Demmer, P.; Fowler, M.; Marino, A. A. Use of Carbon Fibers in the Reconstruction of Knee Ligaments. *Clin. Orthop. Relat. Res.* **1991**, *271* (271), 225–232.

(67) Aoki, K.; Usui, Y.; Narita, N.; Ogiwara, N.; Iashigaki, N.; Nakamura, K.; Kato, H.; Sano, K.; Ogiwara, N.; Kametani, K.; Kim, C.; Taruta, S.; Kim, Y. A.; Endo, M.; Saito, N. A Thin Carbon-Fiber Web as a Scaffold for Bone-Tissue Regeneration. *Small* **2009**, *5* (13), 1540–1546. https://doi.org/10.1002/smll.200801610.

(68) Baur, J. E.; Kristensen, E. W.; May, L. J.; Wiedemann, D. J.; Wightman, R. M. Fast-Scan Voltammetry of Biogenic Amines. *Anal. Chem.* **1988**. https://doi.org/10.1021/ac00164a006.

(69) Howell, J. O.; Kuhr, W. G.; Ensman, R. E.; Mark Wightman, R. Background Subtraction for Rapid Scan Voltammetry. *J. Electroanal. Chem.* **1986**. https://doi.org/10.1016/0022-0728(86)80187-5.

(70) Liu, Y.; Zou, X.; Dong, S. Electrochemical Characteristics of Facile Prepared Carbon Nanotubes-Ionic Liquid Gel Modified Microelectrode and Application in Bioelectrochemistry. *Electrochem. commun.* **2006**. https://doi.org/10.1016/j.elecom.2006.06.024.

(71) Gerhardt, G. A.; Oke, A. F.; Nagy, G.; Moghaddam, B.; Adams, R. N. Nafion-Coated Electrodes with High Selectivity for CNS Electrochemistry. *Brain Res.* **1984**. https://doi.org/10.1016/0006-8993(84)90963-6.

(72) Witkowski, A.; Brajter, A. T. Overoxidized Polypyrrole Films: A Model for the Design of Permselective Electrodes. *Anal. Chem.* **1992**. https://doi.org/10.1021/ac00030a012.

(73) Pihel, K.; Walker, Q. D.; Wightman, R. M. Overoxidized Polypyrrole-Coated Carbon Fiber Microelectrodes for Dopamine Measurements with Fast-Scan Cyclic Voltammetry. *Anal. Chem.* **1996**. https://doi.org/10.1021/ac960153y.

(74) Gonon, F. G.; Fombarlet, C. M.; Buda, M. J.; Pujol, J. F. Electrochemical Treatment of Pyrolytic Carbon Fiber Electrodes. *Anal. Chem.* **1981**. https://doi.org/10.1021/ac00232a020.

(75) Kovach, P. M.; Deakin, M. R.; Wightman, R. M. Electrochemistry at Partially Blocked

Carbon-Fiber Microcylinder Electrodes. *J. Phys. Chem.* **1986**. https://doi.org/10.1021/j100410a028.

(76) Salazar, P.; Martín, M.; González-Mora, J. L. Polydopamine-Modified Surfaces in Biosensor Applications. *Polym. Sci. Res. Adv. Prat. Appl. Educ. Asp.* **2007**.

(77) Laurila, T.; Sainio, S.; Caro, M. Hybrid Carbon Based Nanomaterials for Electrochemical Detection of Biomolecules. *Progress in Materials Science*. 2017. https://doi.org/10.1016/j.pmatsci.2017.04.012.

(78) Swamy, B. E. K.; Venton, B. J. Carbon Nanotube-Modified Microelectrodes for Simultaneous Detection of Dopamine and Serotonin in Vivo. *Analyst* **2007**. https://doi.org/10.1039/b705552h.

(79) Hočevar, S. B.; Wang, J.; Deo, R. P.; Musameh, M.; Ogorevc, B. Carbon Nanotube Modified Microelectrode for Enhanced Voltammetric Detection of Dopamine in the Presence of Ascorbate. *Electroanalysis* **2005**. https://doi.org/10.1002/elan.200403175.

(80) Wildgoose, G. G.; Banks, C. E.; Leventis, H. C.; Compton, R. G. Chemically Modified Carbon Nanotubes for Use in Electroanalysis. *Microchimica Acta*. 2006. https://doi.org/10.1007/s00604-005-0449-x.

(81) Zhang, M.; Liu, K.; Xiang, L.; Lin, Y.; Su, L.; Mao, L. Carbon Nanotube-Modified Carbon Fiber Microelectrodes for in Vivo Voltammetric Measurement of Ascorbic Acid in Rat Brain. *Anal. Chem.* **2007**. https://doi.org/10.1021/ac0705871.

(82) Brett, C. M. A.; Brett, A. M. O. *Electrochemistry: Principles, Methods and Application*; Oxford University Press: Midsomer Norton, 1993.

(83) Elgrishi, N.; Rountree, K. J.; McCarthy, B. D.; Rountree, E. S.; Eisenhart, T. T.; Dempsey, J. L. A Practical Beginner's Guide to Cyclic Voltammetry. *J. Chem. Educ.* **2018**. https://doi.org/10.1021/acs.jchemed.7b00361.

(84) Katz, E.; Willner, I. Probing Biomolecular Interactions at Conductive and Semiconductive Surfaces by Impedance Spectroscopy: Routes to Impedimetric Immunosensors, DNA-Sensors, and Enzyme Biosensors. *Electroanalysis*. 2003. https://doi.org/10.1002/elan.200390114.

(85) González-Cortés, A. Electrochemical Impedance Spectroscopy. In *Agricultural and Food Electroanalysis*; 2015. https://doi.org/10.1002/9781118684030.ch14.

(86) Randviir, E. P.; Banks, C. E. Electrochemical Impedance Spectroscopy: An Overview of Bioanalytical Applications. *Analytical Methods*. 2013.

https://doi.org/10.1039/c3ay26476a.

(87) Grahame, D. C. The Electrical Double Layer and the Theory of Electrocapillarity. *Chem. Rev.* **1947**. https://doi.org/10.1021/cr60130a002.

(88) Dweik, M.; Stringer, R. C.; Dastider, S. G.; Wu, Y.; Almasri, M.; Barizuddin, S. Specific and Targeted Detection of Viable Escherichia Coli O157:H7 Using a Sensitive and Reusable Impedance Biosensor with Dose and Time Response Studies. *Talanta* **2012**. https://doi.org/10.1016/j.talanta.2012.02.056.

(89) Nishikata, A.; Ichihara, Y.; Tsuru, T. An Application of Electrochemical Impedance Spectroscopy to Atmospheric Corrosion Study. *Corros. Sci.* **1995**. https://doi.org/10.1016/0010-938X(95)00002-2.

(90) He, Z.; Mansfeld, F. Exploring the Use of Electrochemical Impedance Spectroscopy (EIS) in Microbial Fuel Cell Studies. *Energy and Environmental Science*. 2009. https://doi.org/10.1039/b814914c.

(91) Song, J.; Gao, T.; Miao, X.; Hao, L.; Cai, K. The Impedance Properties Analysis of Composite Electrodes for Supercapacitor. In *Proceedings of the 2015 International Conference on Mechatronics, Electronic, Industrial and Control Engineering*; Atlantis Press: Paris, France, 2015. https://doi.org/10.2991/meic-15.2015.268.

(92) Scientific, T. F. Energy Dispersive X-Ray Microanalysis, An Introduction http://tools.thermofisher.com/content/sfs/brochures/D17000~.pdf.

(93) Vernon-Parry, K. D. Scanning Electron Microscopy: An Introduction. *III-Vs Rev.* **2000**, *13* (4), 40–44. https://doi.org/10.1016/S0961-1290(00)80006-X.

(94) Baradoke, A.; Juodkazyte, J.; Masilionis, I.; Selskis, A.; Pauliukaite, R.; Valiokas, R. Combined Soft Lithographic and Electrochemical Fabrication of Nanostructured Platinum Microelectrode Arrays for Miniaturized Sensor Applications. *Microelectron. Eng.* **2019**, *208*, 39–46. https://doi.org/10.1016/j.mee.2019.02.003.

(95) Baradoke, A.; Hein, R.; Li, X.; Davis, J. J. Reagentless Redox Capacitive Assaying of C-Reactive Protein at a Polyaniline Interface. *Anal. Chem.* **2020**, *92* (5), 3508–3511. https://doi.org/10.1021/acs.analchem.9b05633.

(96) Baradoke, A.; Pastoriza-Santos, I.; González-Romero, E. Screen-Printed GPH Electrode Modified with Ru Nanoplates and PoPD Polymer Film for NADH Sensing: Design and Characterization. *Electrochim. Acta* **2019**, *300*, 316–323. https://doi.org/10.1016/j.electacta.2019.01.128.

(97) Baradoke, A.; Jose, B.; Pauliukaite, R.; Forster, R. J. Properties of Anti-CA125 Antibody Layers on Screen-Printed Carbon Electrodes Modified by Gold and Platinum Nanostructures. *Electrochim. Acta* **2019**, *306*, 299–306. https://doi.org/10.1016/j.electacta.2019.03.081.

(98) Baradoke, A.; Santos, A.; Bueno, P. R.; Davis, J. J. Introducing Polymer Conductance in Diagnostically Relevant Transduction. *Biosens. Bioelectron.* **2021**, *172*, 112705. https://doi.org/10.1016/j.bios.2020.112705.

(99) Shrivastava, A.; Gupta, V. Methods for the Determination of Limit of Detection and Limit of Quantitation of the Analytical Methods. *Chronicles Young Sci.* **2011**, *2* (1), 21. https://doi.org/10.4103/2229-5186.79345.

PUBLISHED CONTRIBUTIONS TO ACADEMIC CONFERENCES

1. Jafarov, Ali; Merzlikin, Mark; Elsakova, Alexandra; Baradoke, Ausra (2021). 3D printed electrochemical cells for biosensing on flexible carbon electrodes. *XXVIth International Symposium on Bioelectrochemistry and Bioenergetics of the Bioelectrochemical Society", Romania, Cluj-Napoca, 9–13th of May 2021*. Bioelectrochemistry.
2. Elsakova, Alexandra; Merzlikin, Mark; Jafarov, Ali; Baradoke, Ausra (2021). Development of an electrochemical biomarker detection based on non-modified disposable carbon electrodes. *XXVIth International Symposium on Bioelectrochemistry and Bioenergetics of the Bioelectrochemical Society", Romania, Cluj-Napoca, 9–13th of May 2021*. Bioelectrochemistry.

NON-EXCLUSIVE LICENCE TO REPRODUCE THESIS

I,_____ Mark Merzlikin_____,

(*author's name*)

1. herewith grant the University of Tartu a free permit (non-exclusive licence) to:

1.1. reproduce, for the purpose of preservation, including for adding to the DSpace digital archives until the expiry of the term of copyright, and

1.2. make available to the public via the web environment of the University of Tartu, including via the DSpace digital archives, under the Creative Commons licence CC BY NC ND 3.0, which allows, by giving appropriate credit to the author, to reproduce, distribute the work and communicate it to the public, and prohibits the creation of derivative works and any commercial use of the work from ***21/05/2023*** until the expiry of the term of copyright,

_____Electrochemical sensing on flexible carbon electrodes for applications in _____ soft robotics__ _____ _____,

(*title of thesis*)

supervised by _____Dr. Janno Torop, Dr. Aušra Baradoke _____,

(*supervisor's name*)

2. I am aware of the fact that the author retains the rights specified in p. 1.

3. I certify that granting the non-exclusive licence does not infringe other persons' intellectual property rights or rights arising from the personal data protection legislation.

Mark Merzlikin

21/05/2021